THESIS

FATIGUE AND RUTTING ANALYSES OF A PAVEMENT STRUCTURE WITH EXPANSIVE SOIL-RUBBER (ESR) BASE STABILIZED WITH OFF-SPECIFICATION FLY ASH

Submitted by

Emily L. Budagher

Department of Civil and Environmental Engineering

In partial fulfillment of the requirements

For the Degree of Master of Science

Colorado State University

Fort Collins, Colorado

Fall 2012

Master's Committee:

Advisor: J. Antonio H. Carraro

Charles D. Shackelford
Loren G Funk

ABSTRACT

FATIGUE AND RUTTING ANALYSES OF A PAVEMENT STRUCTURE WITH EXPANSIVE SOIL-RUBBER (ESR) BASE STABILIZED WITH OFF-SPECIFICATION FLY ASH

The focus of this study is to analyze through resilient modulus testing and computer simulations the feasibility of an expansive soil-rubber (ESR) mixture stabilized with off-specification fly ash (ESR-FA) as a pavement base layer. Three mixtures were tested in this study, which were expansive soil, ESR, and ESR-FA mixtures. The off-specification fly ash used included a high sulfur content. The ESR mixture consisted of high-plasticity clay blended with 20% 6.7-mm granulated rubber (by weight). The ESR-FA consisted of the same high-plasticity clay blended with 20% 6.7-mm granulated rubber (by weight) and 14% fly ash. All mixtures were tested at a target relative compaction level equal to 95% (±0.5%) of the Standard Proctor maximum dry density. Expansive soil and ESR specimens were subjected to resilient modulus and Poisson's ratio testing immediately after compaction. ESR-FA specimens were allowed to cure for 14 days before being subjected to resilient modulus and Poisson's ratio testing. All specimens were unsaturated during testing. Stiffness changes due to scrap tire rubber addition and fly ash addition were evaluated during resilient modulus testing. Poisson's ratio was determined using axial and radial transducers during unconfined compression testing. Results suggest that the stiffness of the expansive soil specimen is significantly greater than that of the ESR and ESR-FA specimens. However, the stiffness of the ESR-FA specimen is greater than that of the ESR specimen, which makes it a medium between the expansive soil specimen and the ESR specimen.

ACKNOWLEDGEMENTS

Professor Antonio Carraro deserves special acknowledgement for the support and guidance during coursework, research, and preparation of the thesis. Thanks to Professors Charles Shackelford and Loren Funk for support on the graduate committee. A special thanks to professors Antonio Carraro, Charles Shackelford, and Paola Bandini for being outstanding teachers.

A special acknowledgement to the author's parent's and stepdad William Budagher, Jenny, and Chris Morton. To the author's sisters Katie Budagher and Amanda Quillin. A special acknowledgement to the rest of the author's family for their support and encouragement.

The United States Department of Transportation - Mountain-Plains Consortium (USDOT-MPC) partially funded this research. Rawhide Energy Station provided the fly ash, and Caliber Recycled Products Inc. provided the scrap tire rubber. Their contributions are appreciated.

TABLE OF CONTENTS

LIST OF TABLES

LIST OF FIGURES

LIST OF ACRONYMS

AASHTO ..... American Association of State Highway and Transportation Officials
ACAA ..... American Coal Ash Association
ASTM ..... American Society for Testing and Materials
CBR ..... California Bearing Ratio
CCP ..... Coal Combustion Product
CDPHE ..... Colorado Department of Public Health and Environment
CH ..... High Plasticity Clay
CSU ..... Colorado State University
EPA ..... Environmental Protection Agency
ESR ..... Expansive Soil-Rubber
FAC ..... Fly Ash Content
FESEM ..... Field Emission Scanning Electron Microscope
FGD ..... Flue Gas Desulfurization
MPC ..... Mountain Plains Consortium
R ..... Rawhide
RC ..... Rubber Content
RMA ..... Rubber Manufacturers Association
SEM ..... Scanning Electron Microscope
STR ..... Scrap Tire Rubber
USCS ..... Unified Soil Classification System

CHAPTER 1. INTRODUCTION

1.1 Problem Statement

Expansive soils can be found in every state and cover about one-fourth of the United States (Pupalla and Cerato 2009). The Front Range of Colorado has significant amounts of expansive soils, which are geomaterials that undergo substantial volume changes when subjected to variations in water content. These volume changes or shrink-swell cycles are typically non-uniform and produce large ground movements causing significant damage to public and private structures through cracking and buckling. Annual losses caused by the damage of expansive soils result in billions of dollars (Pupalla and Cerato 2009). The cost of damage to homes due to expansive soil was reported to be $13 billion per year (Pupalla and Cerato 2009). The presence of expansive soils in the Front Range of Colorado and throughout the world has brought forth the need for further geotechnical analysis, such as the effects of the addition recyclable materials, in order to minimize the swell potential and effects of heave on structures.

Scrap tires could provide a potential solution for this problem. The Colorado Department of Public Health and Environment reported that there were 4,829,711 tires generated in the state of Colorado in 2010. Of the 4,829,711 tires that were generated, 4,485,777 tires were recycled, which amounts to about 93% of the total (CDPHE 2010). The remaining 7% were stored at waste tire facilities, increasing the total number of waste tires in storage to about 57 million (CDPHE 2010). This excessive amount of scrap tires has created the need to uncover and implement new uses for scrap tire rubber (STR).

Less than about 5.5% of the STR generated in the United States is used in civil engineering projects (Rubber Manufacturers Association 2012). Some examples of civil engineering projects that use STR are embankment fills, retaining walls, and asphalt/sealant. Research studies have been conducted on sand-rubber mixtures (Ahmed & Lovell 1993; Lee et al. 1999; Lee et al. 2007; Kim & Santamarina 2008) and on clay-rubber mixtures (Ozkul and Baykal 2001) in order to further the uses of these mixtures in civil engineering applications.

Seda et al. (2007) conducted research on expansive soil and rubber (ESR) mixtures and found that the swell potential and swell pressure of untreated expansive soil is reduced with the addition of STR. Research conducted by Dunham-Friel (2009) also found that the addition of STR reduces the swell potential and swell pressure of expansive soil. However, Dunham-Friel also found that ESR specimens have significantly lower stiffness than expansive soil specimens. Research conducted by Wiechert (2011) showed that the stiffness of ESR mixtures that are properly designed and stabilized with off-specification fly ash (ESR-FA) could be restored to the stiffness values observed for compacted, untreated soil. Therefore, the next step towards implementation of the technology in practice involves carrying out a systematic parametric study to simulate the performance of the proposed technology in specific civil engineering applications. The focus of this study is to analyze through resilient modulus testing and computer simulations the feasibility of an ESR mixture stabilized with off-specification fly ash as a pavement base layer.

1.2 Research Objectives

The broad objective of this research is to synthetically evaluate the performance of ESR mixtures stabilized with off-specification fly ash as a pavement base layer using a computer program.

The specific objectives of this study are to:

1. conduct resilient modulus (M_r) tests on a select ESR mixture stabilized with off-specification fly ash (ESR-FA);
2. assess the Poisson's ratio tests of expansive soil, ESR, and ESR-FA mixtures; and
3. evaluate the performance of pavement base layers of expansive soil, ESR, and ESR-FA using a computer program.

1.3 Research Scope

This study was carried out using a single source of expansive soil, rubber, and fly ash for the expansive soil, ESR, and ESR-FA mixtures tested. The rubber content (*RC*), which is defined as the ratio of the dry mass of rubber to the dry mass of rubber and soil for ESR mixtures, or the ratio of the dry mass of rubber to the dry mass of rubber, soil, and fly ash for ESR-FA mixtures, was equal to 20% for all ESR and ESR-FA specimens tested. The fly ash content (*FAC*), which was defined as the ratio of the dry mass of fly ash to the dry mass of fly ash and soil, was equal to 14% for all ESR-FA specimens tested. These parameters are consistent with the RC and FAC used in a previous study with similar materials (Wiechert 2011).

Expansive soil, ESR, and ESR-FA specimens were statically compacted according to the AASHTO T 307 specification with a relative compaction (C_R) equal to 95% of the standard

Proctor maximum dry density and standard Proctor optimum water content (w_{opt}). The relative compaction and optimum water content were determined for each mixture according to ASTM D 698. Expansive soil, ESR, and ESR-FA specimens were subjected to resilient modulus and Poisson's ratio testing. All expansive soil and ESR specimens were tested immediately after compaction. ESR-FA specimens were compacted 1 to 2 hours after the addition of fly ash, and then were allowed to cure for either 7 or 14 days before testing.

The resilient modulus and Poisson's ratio values determined for expansive soil, ESR, and ESR-FA specimens were subsequently used as design parameters in the computer simulations carried out using the Weslea for Windows software to evaluate three types of pavement structures, namely:

1. Asphalt concrete placed directly on an expansive soil subgrade,
2. Asphalt concrete, ESR base, and expansive soil subgrade, or
3. Asphalt concrete, ESR-FA base, and expansive soil subgrade.

Four base thicknesses were evaluated for each of the three pavement structures listed above, which were:

1. 10.16 cm (4 in)
2. 20.32 cm (8 in)
3. 30.48 cm (12 in)
4. 40.64 cm (16 in)

1.4 Manuscript organization

This manuscript is organized into six chapters, which present the literature background of the research, the research approach followed to complete the research objectives, and the analyses of the results found. A more detailed description of the chapters is as follows:

- Chapter 1 introduces the problems associated with expansive soils, and the excessive amount of STR.
- Chapter 2 summarizes the existing literature on the materials used in the experimental program as well as past research that has been conducted that is related to the objectives of this study.
- Chapter 3 presents the conceptual framework used to analyze data attained from laboratory testing, and a detailed analysis of the software used for the computer simulations.
- Chapter 4 describes the experimental framework used in the preparation of the expansive soil, ESR, and ESR-FA specimens, and all the tests that were conducted on them.
- Chapter 5 presents an analysis of the results obtained from the resilient modulus tests, Poisson's ratio tests, and the computer simulations.
- Chapter 6 concludes this study by summarizing the results and suggesting future work needed.

CHAPTER 2. LITERATURE REVIEW

2.1 Expansive Soil

Expansive soil deposits are located throughout the world. Figure 2.1 is a map of the expansive soil deposits found in the United States. This map shows that expansive soils are located from the Gulf of Mexico to Canada. There are also some expansive soil deposits along the West Coast.

The Front Range of Colorado has significant deposits of expansive soils. This area also happens to be the location of many of Colorado's cities including Denver, the largest city in Colorado. The presence of expansive soils in conjunction with improper engineering design, in the Front Range has caused damage to private and commercial structures, which has brought forth the need for further geotechnical analysis in order to minimize the swell potential and effects of induced movements on a proposed structure.

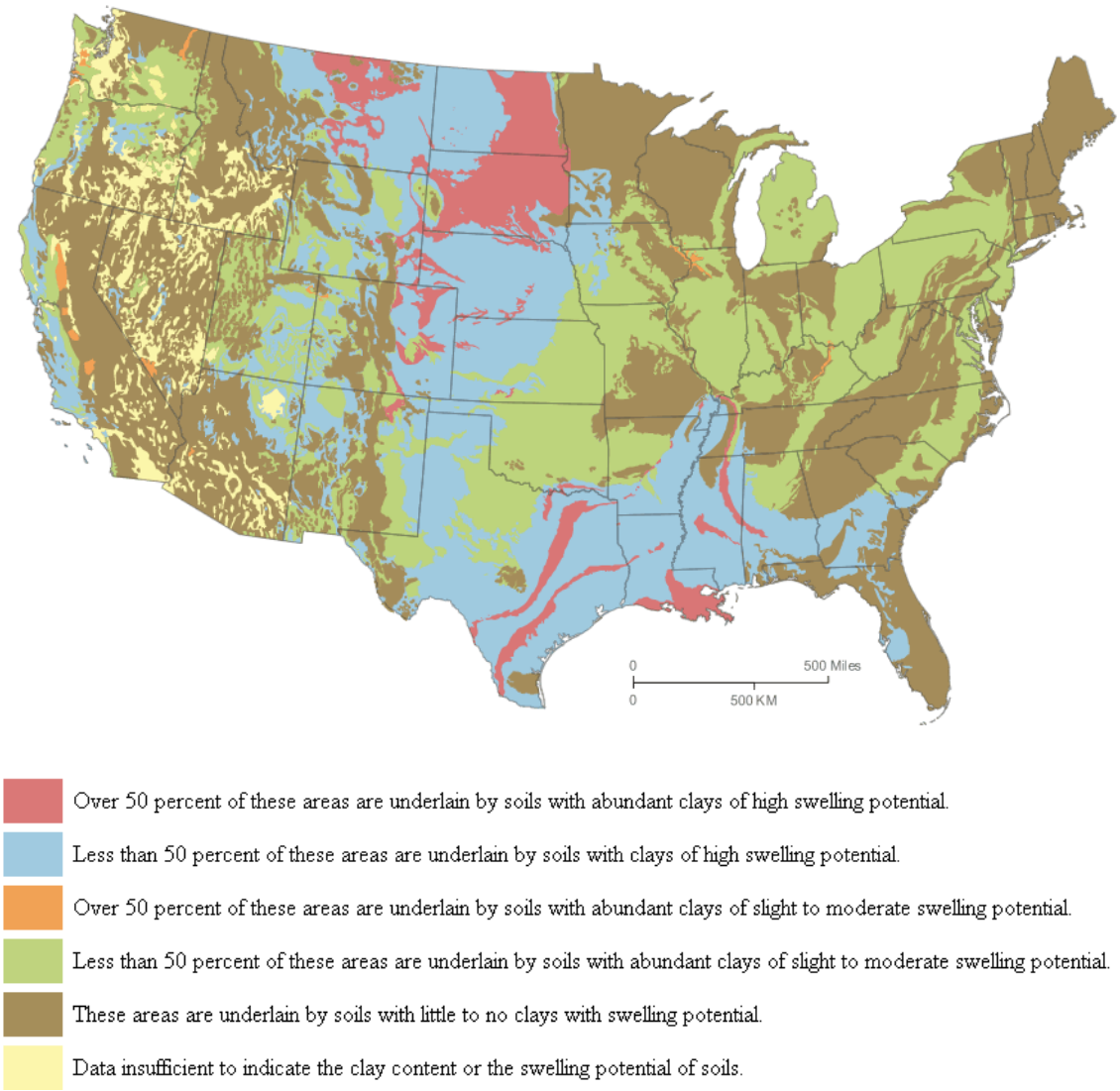

Figure 2.1: United States Map of Expansive Soil Locations (Olive, et al. 1989)

2.2 Scrap Tire Rubber

A potential solution for the problem of expansive soils could be provided by scrap tires (Seda et al. 2007). The Colorado Department of Public Health and Environment (CDPHE) reported that there were 4,829,711 tires generated in the state of Colorado in 2010. Of the 4,829,711 tires that were generated, 4,485,777 were recycled, which amounts to about 93% of the total (CDPHE 2010). The remaining 7% were stored at waste tire facilities, increasing the total number of tires stored in waste tire monofills to 57,361,045. The total number of waste tires stored temporarily at

waste tire processing facilities increased to 4,832,830 in the year 2010 (CDPHE 2010). Figure 2.2 is a graph of the Colorado 2010 waste tire inventory estimate. According to the Rubber Manufactures Association's *Scrap Tire Markets in the United States* report, Colorado contains the largest stockpile of tires for storage in the country.

Figure 2.2: Colorado 2010 Waste Tire Inventory Estimate (CDPHE 2010)

Rubber Manufactures Association's *Scrap Tire Markets in the United States* reported that 4105.8 thousand tons (89% of scrap tires generated in 2007) of scrap tires were consumed in end use markets throughout the Unites States in 2007, and estimated that 4595.7 thousand tons of scrap tires were generated in 2007. In Colorado alone, nearly 50 million scrap tires sit in stockpiles (Rubber Manufactures Association 2009).

Scrap tire stockpiles can catch fire from lightning strikes, equipment malfunctions, or arson, which can cause air, surface water, soil, groundwater, and residual contamination, making them hazardous to the human, animal, and plant life (U.S. EPA 2006). Figure 2.3 is a photograph taken by Todd Thalhamer of a scrap tire stockpile located in California that has caught fire. Stockpiles are also hazardous to human health because they provide warm, protected, stagnant water, creating breeding grounds for mosquitoes, which transmit deadly diseases such as dengue fever, encephalitis, and the West Nile virus (U.S. EPA 2006).

Figure 2.3: Photograph of Waste Scrap Tires on Fire (U.S. EPA 2006)

This excess amount of tires has created the need to uncover and implement new uses for scrap tire rubber (STR). According to Figure 2.4 approximately 5.5% of the STR generated in the United States is used in civil engineering projects (Rubber Manufaccturers Association 2009).

Figure 2.5 shows that approximately 2.2% of the STR generated in region VIII classified by the EPA are used in civil engineering projects (RMA 2006). Region VIII consists of Colorado, Montana, North Dakota, South Dakota, Utah, Wyoming and 27 Tribal Nations (RMA 2006). Some examples of civil engineering projects that use STR are large highway embankment or lightweight fill projects (U.S. EPA 2006). These projects can consume up to 1,500,000 tires per project (U.S. EPA 2006). STR is also used in landfill applications such as daily cover, leachate collection layers, surface water drainage layers, and gas collection channels (U.S. EPA 2006).

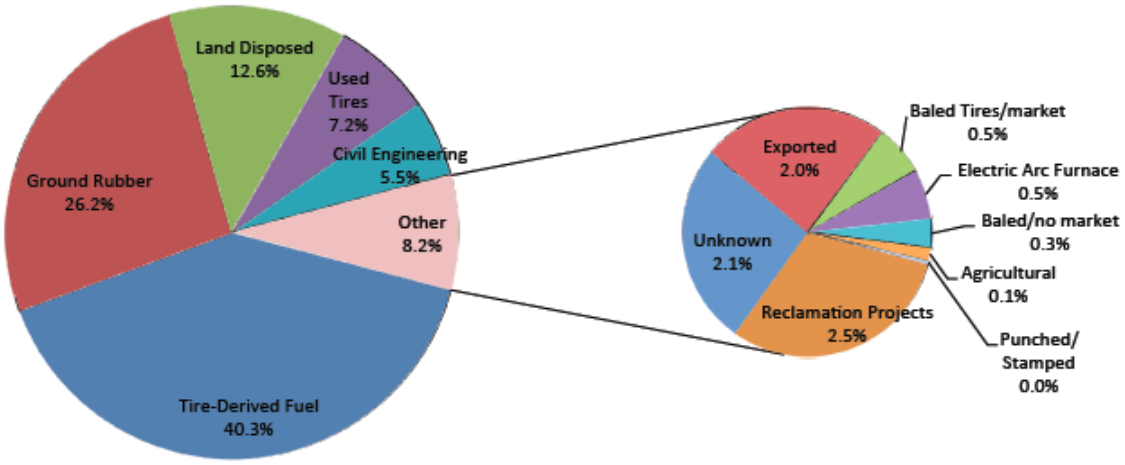

Figure 2.4: 2009 U.S. Scrap Tire Disposition (Rubber Manufaccturers Association 2009)

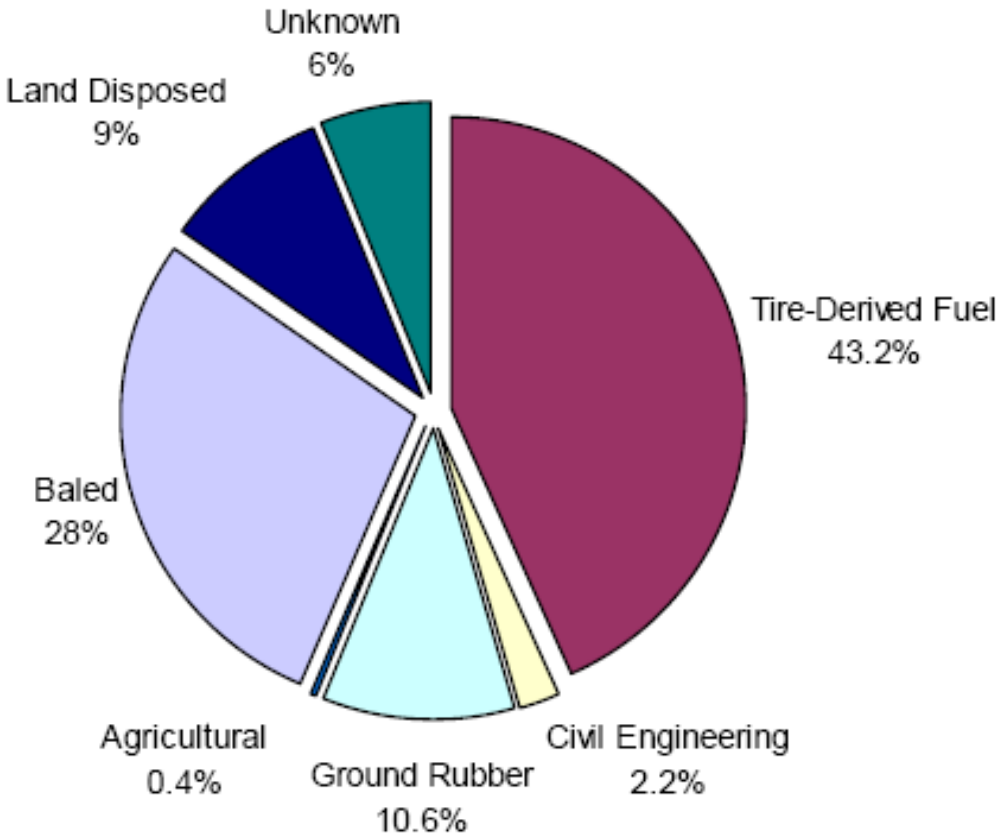

Figure 2.5: United States EPA region VIII scrap tire rubber markets (RMA 2006)

2.3 Soil-Rubber Mixtures

Some examples of civil engineering projects that use STR are embankment fills, retaining walls, and asphalt/sealant. Research studies have been conducted on sand-rubber mixtures (Ahmed & Lovell 1993; Lee et al. 1999; Lee et al. 2007; Kim & Santamarina 2008), and on clay-rubber mixtures (Ozkul and Baykal 2001, Seda et al. 2007, Dunham-Friel 2009) in order to further the uses of these mixtures in civil engineering applications. In this study, focus is placed on clay-rubber mixtures, particularly those involving expansive soils.

2.3.1 Clay-Rubber Mixtures

Ozkul and Baykal (2001) evaluated the drained and undrained shear strength of clay mixtures and tire buffings. The clay evaluated was a kaolinite rich clay with a liquid limit of 32% and a plastic limit of 23%. Approximately 43% of the soil was clay and the remanding soil was silt. The tire buffings or rubber fibers used were a by-product of the tire retread process, which had particle sizes varying from 2 to 25 mm in length and 0.3 3.6 mm in diameter.

The two soil mixtures evaluated were kaolinitic clay (K) and kaolinitic clay mixed with 10% (by dry weight) rubber fibers. The mixtures were prepared at 1 to 2% wet of their optimum values at Standard (ASTM D698) and Modified (ASTM D1557) compaction efforts. The specimen size was 7 cm in diameter and 15 cm in height. Standard triaxial tests were conducted at effective confining stresses ranging from 50 to 300 kPa. Specimens were consolidated until pore pressure equalization was confirmed, and then permeability tests were conducted. Consolidated-drained (CD) and consolidated-undrained (CU) tests were conducted, and both CD and CU tests samples were sheared to 20% strain. Also, postshear permeability tests were conducted. Pressures (cell pressure, backpressure, and drainage pressure), load, deformation and volume changes of the test specimen during all stages of testing were recorded by an automatic data acquisition and logging system.

This study showed that the peak strength of the composite was comparable to or greater than that of the clay alone when tested at confining stresses below 200-300 kPa under conditions of full saturation in either drained or undrained testing. However, the composite tended to degrade the strength of the clay for confining stresses above that threshold. The average hydraulic

conductivity was around 2 x 10-7 cm/s for the clay alone, and did not change significantly with the addition of rubber fibers.

Although the research conducted by Ozkul and Baykal (2001) shows the potential of clay-rubber mixtures. There are other studies that have been conducted on local soils found in the Front Rage region of Colorado that are more pertinent to this study. Seda et al. (2007) have conducted such studies.

Seda et al. (2007) conducted research on expansive soil and expansive soil with a rubber content (*RC*) equal to 20% by weight. The expansive soil used belonged to the Mancos shale formation and was classified according to the Unified Soil Classification System (USCS) as CH. The STR particles ranged from 2.0 to 6.7 mm. The expansive soil-rubber mixtures (ESR) were classified as CH according to USCS. Seda conducted index tests such as specific gravity, Atterberg limits, grain-size distribution, and water content vs. dry unit weight as well as compaction, and one-dimensional swell-consolidation tests on both the expansive soil and the ESR mixtures. The specimens evaluated in the swell-consolidation tests were prepared close to 100% of standard Proctor maximum dry density and at the optimum water content, and were inundated with water under a vertical stress of 6.1 kPa.

The Atterberg limits and plasticity indices of the soil and ESR mixture were similar. This was due to the fact that less than 0.4% by weight of waste tire rubber passed sieve No. 40. The specific gravities of the expansive soil and the ESR mixtures were 2.81 and 2.16. The expansive soil and ESR water contents were the same, but the maximum dry unit weight of the ESR

mixture was less than the expansive soil maximum dry unit weight. The swell potential and swell pressure were reduced by approximately 49% and 75% respectively with the addition of 20% waste tire rubber by weight, and the compression and recompression indices increased by 24% and 57% with the addition of 20% waste tire rubber. In conclusion, the addition of rubber reduces swell potential and swell pressure, but it increases compressibility, which means that ESR mixtures may be used to reduce the amount of heave cause by expansive soil as long as the compressibility of the ESR mixture is taken into account. Seda (2007) proposed that ESR mixtures could be used as backfill materials for residential foundations, retaining walls, or highway bridge abutments.

Seda et al. (2007) showed that the swell potential and swell pressure could be reduced with the addition of STR. However, the strength and stiffness characteristics still need to be analyzed in order to better understand if the ESR mixtures could be used for civil engineering applications.

Dunham-Friel (2009) investigated further into the effects of STR addition to expansive soil. He stated that in order to consider using ESR mixtures in geotechnical applications it was critical to thoroughly understand the strength and stiffness characteristics of ESR mixtures relative to expansive soil alone. The expansive soil used in this study was a Pierre shale residual soil from the Front Range of Colorado, and is classified as CH (highly plastic inorganic clay) according to USCS. The granulated rubber, which was manufactured by Caliber Recycled Products in Commerce City, Colorado, had a maximum particle size of 6.7 mm. The ESR mixtures tested contained rubber contents equal to 10% and 20%. All specimens were prepared to a target

relative compaction equal to 95% and optimum water content. These two compaction parameters were based on the standard Proctor compaction curves of each mixture.

The shear strength and stiffness of the expansive soil and the ESR mixtures were evaluated using undrained axisymmetric compression. The mechanical response of all the specimens was characterized according to two variable changes, which were rubber content and mean effective confining stress. Compacted specimens were isotropically consolidated at mean effective stresses of 50, 100 and 200 kPa, and sheared in undrained axisymmetric compression to axial strain equal to 27%. Bender element tests were conducted at mean effective stresses of 50, 100 and 200 kPa in order to determine the small-strain stiffness of the expansive soil and ESR mixtures.

Dunham (2009) found that the addition of rubber reduced the amount of phase transformation and/or eliminated undrained stability. Increasing the amount of rubber added also increased the slope of the critical-state lines and the critical-state friction angles. However, for all three levels of mean effective stress, the increase in rubber content decreased both the large strain stiffness and the small strain stiffness. The ESR mixture's maximum shear modulus was approximately 44% to 63% less than that of the expansive soil maximum shear modulus.

In conclusion, the ESR mixtures were stronger than the expansive soil, but the material stiffness of the ESR mixtures was less than the material stiffness of the expansive soil. Dunham suggested that ESR mixtures could be used in applications where material stiffness is not a primary concern, such as backfills of retaining or foundation walls.

However, for applications where stiffness is a concern, the addition of fly ash is a possibility for improving the stiffness characteristic of ESR mixtures.

2.4 Coal Combustion Products & Fly Ash

Coal combustion products (CCPs) are materials produced by coal-fueled power plants, and they include fly ash, bottom ash, boiler slag, flue gas desulfurization gypsum, and other products (American Coal Ash Association 2010) (American Coal Ash Association Education Foundation 2008). Fly ash is a fine, powdery substance that would fly out of the power plant's stack if it were not captured by the emission control systems at the power plant (American Coal Ash Association Education Foundation 2008). Bottom ash is a course, granular material that collects at the bottom of the coal furnace (American Coal Ash Association Education Foundation 2008). Boiler slag is a black, granular material that is formed in slag tap boilers, and flue gas desulfurization gypsum is produced by emission control systems that remove sulfur and oxides from power plant flue gas streams (American Coal Ash Association 2008). Figure 2.6 displays an example of a steam generating system where CCPs are created. CCPs have have come to be implemented as geomaterials in construction applications such as transportation construction and environmental industries because of their desirable properties and low concentrations of leach contaminants (Ash at Work 2006). Figure 2.7 displays the top uses for CCPs in 2003.

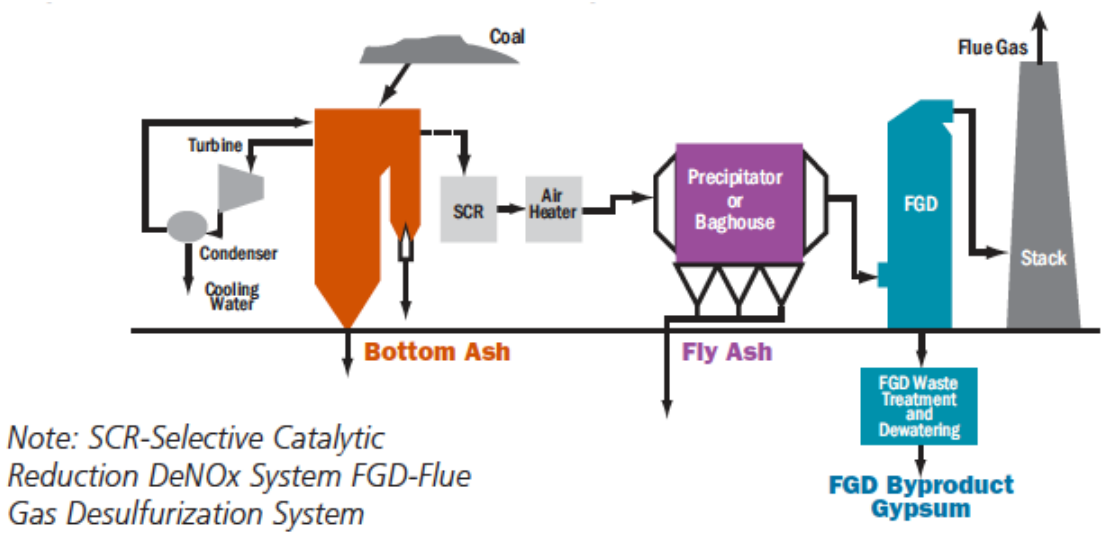

Figure 2.6: Example of Steam Generating System (U.S. Environmental Protection Agency 2005)

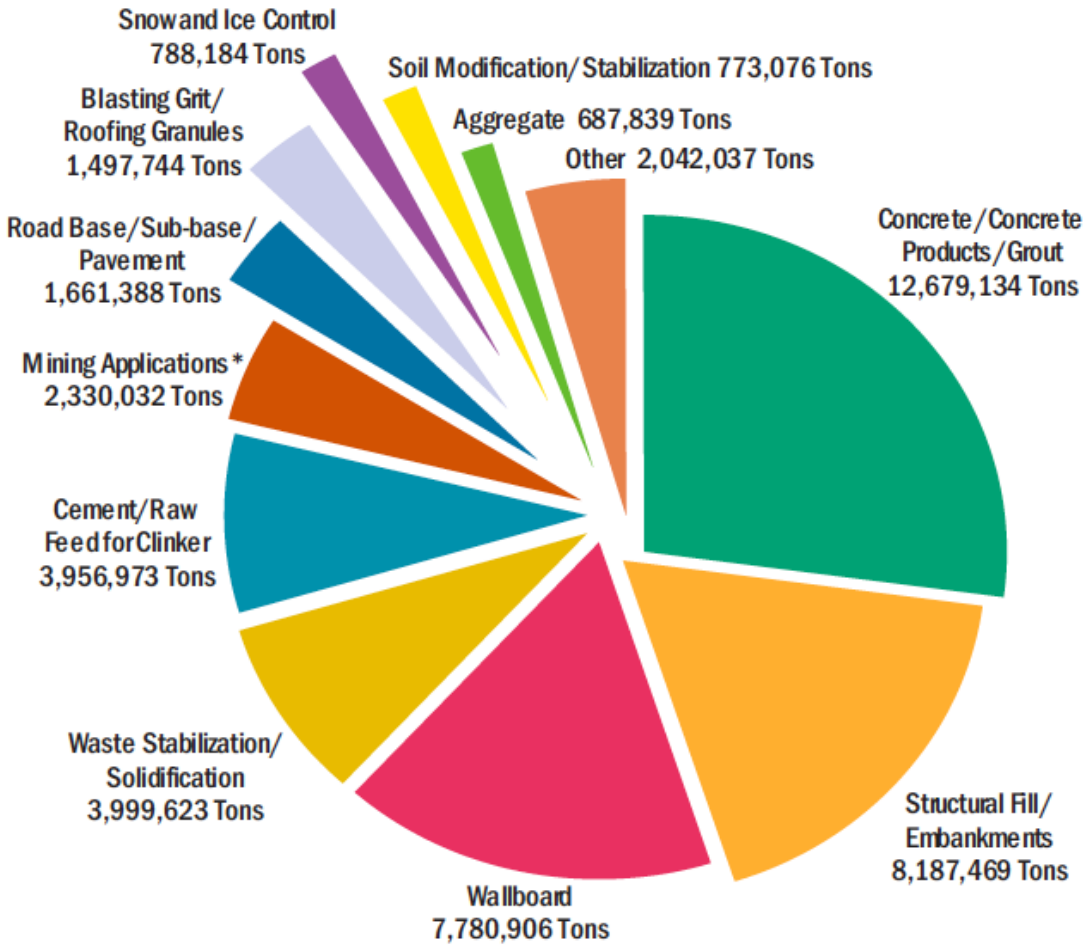

Figure 2.7: Top Uses for CCPs in 2003 (U.S. Environmental Protection Agency 2005)

Fly ash can be classified as Class F, Class C, or off-specification fly ash. ASTM C 6181 distinguishes between Class F and Class C fly ashes based on the sum of the weight percentage of oxides of silicon (SiO_2), aluminum (Al_2O_3) and iron (Fe_2O_3) or S+A+F[1, 2] (Ash at Work 2007). In order to be classified as Class F, the fly ash has to contain at least 70% S+A+F, and a minimum of 50% S+A+F to be classified as Class C (Ash at Work 2007). Both bituminous and anthracite coal (high-rank coal) produce Class F fly ash, and Class C fly ash is produced from sub-bituminous and lignite coal (low-rank coal) (Ash at Work 2007). Class C fly ash must contain above 20% lime content in order to be cementitious (Ash at Work 2007). Off-specification fly ashes are those that don't meet the qualifications of Class F or Class C fly ashes and typically contain high SO3 content or high loss on ignition (LOI).

Fly ash can be used for soil stabilization, mineral fillers for paints, as well as in various agricultural applications. The largest application for fly ash is the production of concrete (American Coal Ash Association 2008). However, off-specification fly ash is not recommended for use in concrete and is more often disposed of. Even though off-specification fly ashes are not recommended for use in concrete, they have been used for soil stabilization. Richard Meininger (U.S. Environmental Protection Agency 2008), a highway research engineer at the Federal Highway Administration, explained the types of fly ash and the problems associated with high-carbon ash (off-specification): He recommends that this type of fly ash be used as a supplementary cementitious material in concrete not only for reasons of durability and economy, but also to help reach environmental goals. Meininger explains that off-specification fly ashes resemble some Class C fly ashes in that they have self-hardening properties when exposed to moisture. Because these fly ashes contain such a high level of carbon, however, they are often

not considered for various projects because the carbon tends to absorb the air-entraining admixture in freshly mixed concrete. This results in problems controlling the entrained air. In spite of this, Meininger believes that it is important to find ways to use non-specification fly ashes in highway construction because they are already heat-treated cementitious materials that have potential environmental and economic benefits (U.S. Environmental Protection Agency 2008). Other application of fly ash can be seen below in Figure 2.8.

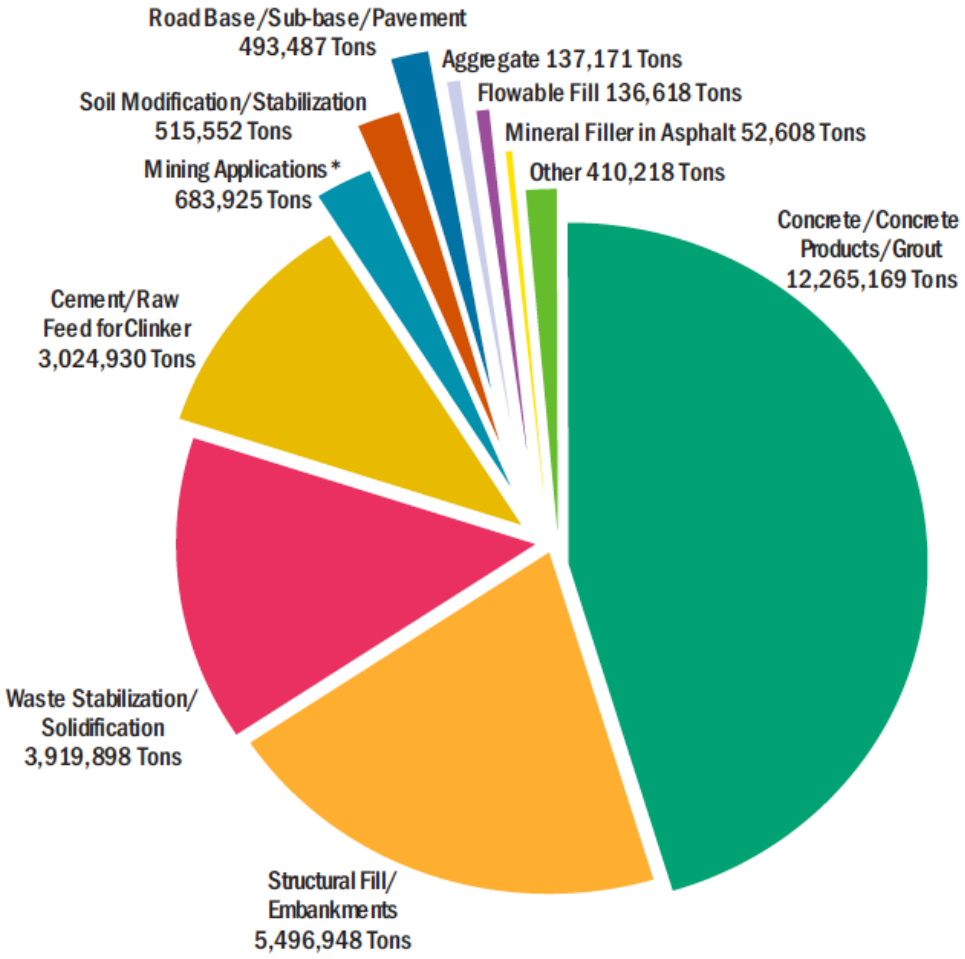

Figure 2.8: Top Uses for Coal Fly Ash in 2003 (U.S. Environmental Protection Agency 2005)

CCPs are desirable because they can reduce a project's carbon footprint. Fly ash alone has greatly contributed to reducing the amount of carbon dioxide that is released into the atmosphere

by replacing cement. For example, for every ton of fly ash used instead of portland cement, approximately one ton of carbon dioxide is prevented from entering the atmosphere (American Coal Ash Association Education Foundation 2008). In 2009, approximately 134,699,739 tons of coal combustion products were produced, while 55,614,563 tons were beneficially used, creating a utilization rate of 41.3% (American Coal Ash Association 2010). The amount of fly ash produced in 2009 was 63,000,000 tons; the amount of fly ash beneficially used was 24,716,665 tons (American Coal Ash Association 2010). The utilization rate for fly ash was 39.2% (American Coal Ash Association 2010).

2.5 Fine-Grained-Fly Ash Mixtures

The studies discussed in section 2.5 pertain to the effects of stabilizing soils with fly ash.

Edil et al. (2009) evaluated the effects of stabilizing soft fine-grained soils with self-cementing fly ashes derived from combustion of sub-bituminous coal. The four fly ashes used were Columbia, Edgewater, Dewey, and King. The first three fly ashes listed were produced at power plant in Wisconsin, and the last fly ash was produced at a power plant in Minnesota. The Columbia and Edgewater fly ashes were Class C fly ash, and the Dewey and King fly ashes were off-specification fly ash. Seven soils were used for testing, and all of the soils were fine grained and classified as CL, CH, and OH according to USCS. Six of the soils were inorganic and one soil was organic.

California bearing ratio (CBR) and resilient modulus (*Mr*) tests were conducted on mixtures prepared at optimum water content, at 7% wet of optimum water content, and at 9-18% wet of

optimum water content. Soil mixtures were compacted using standard Proctor effort. Soil specimens were tested immediately after compaction for CBR tests. Soil-fly ash specimens cured at 25^{o}C and 100% relative humidity for 7 days before being subjected to CBR testing and 14 to 56 days before being subjected to resilient modulus testing.

The results of this study show that the CBR of the soil-fly ash mixtures generally increased with increasing fly ash content and decreased with increasing water content. Soil-fly ash mixtures with a fly ash content of 10%, compacted at 7% wet of optimum tended to have a lower resilient modulus than the soil alone compacted at optimum water content. Soil-fly ash mixtures with a fly ash content of 18% had a resilient modulus typically higher than the soil alone compacted at optimum water content. The resilient modulus increased modestly when specimens cured for 7 to 14 days. However, the resilient modulus increased by 20 to 50% for specimens cured between 14 to 56 days. Soil-fly ash mixtures with inorganic soils tended to have a lower CBR and resilient modulus.

In addition, Cokca (2001) investigated the effect of adding lime, cement, high-calcium and low-calcium Class C fly ash to expansive soil. The expansive soil mixture used for this study was 85% kaolinite, 15% bentonite, and 10% water (this mixture was called Sample A). The fly ashes used were produced at Soma and Tuncbilek Thermal Power Plant in Turkey. Samples were prepared by mixing Sample A with a calculated amount of stabilizer. The amounts of stabilizer varied from 0 to 8% for lime and cement and 0 and 25% for Soma and Tuncbilek dry ash by dry weight of the soil.

Grain size distributions, specific gravity, Atterberg limits, activity, swelling potential, and chemical analysis (ASTM C 311) were conducted on all soil-stabilizer mixtures. Specimens used in swelling potential tests were subjected to cure times of no curing, 7 days curing, and 28 days curing.

The results of this study show that the plasticity index, activity, and swelling potential of the samples decreased with increasing stabilizer percent and increasing cure time. A fly ash content of 20% decreased the swell potential to nearly the same swell potential as a lime content of 8%. The optimum fly ash content was near 20%. In conclusion, both high and low-calcium Class C fly ash was recommended for stabilization of expansive soils.

2.6. ESR Mixtures Stabilized with Off-Specification Fly Ash

The previous studies in Section 2.5 discuss the improvements of the addition of fly ash to different soils. However, for this study, the addition of fly ash to ESR mixtures is more applicable. There has been one study conducted by Wiechert (2011) that further analyze the effects of the addition of fly ashes to expansive soil.

Wiechert et al. (2011) researched the potential use of off-specification fly ash to increase the stiffness of ESR mixtures. The study was carried out using a single source of soil and rubber and three different types of fly ash. The soil used was from the Pierre Shale formation and was classified as a high plasticity clay (CH) according to USCS. The granulated rubber was provided by Caliber Recycled Products Inc. and had a nominal maximum particle size of 6.7 mm. One of the three fly ashes tested was a standard Class C (ASTM C 618) and was used as a control fly

ash. Wiechert et al. (2011) stated in their study that Class C fly ash is desirable for soil stabilization because of its pozzolanic and self- cementing characteristics. Fly ash not conforming to ASTM C 618 was referred to as off-specification fly ash. The Class C fly ash was produced at Laramie River Station in Wheatland, Wyoming, and the off-specification fly ashes were produced at Rawhide Energy Station in Fort Collins, Colorado, and Drake Power Plant in Colorado Springs, Colorado. The ESR mixtures were blended with the Laramie fly ash, Rawhide fly ash, and a combination of 40% Drake fly ash and 60% Laramie fly ash.

The rubber content for all the specimens was defined as the ratio of the dry mass of rubber to the dry mass of rubber and soil and was equal to 20%. The fly ash content for all the specimens was defined as the ratio of the dry mass of fly ash to the dry mass of fly ash and soil and was equal to 14%. The fly ash content required to develop pozzolanic reactions was determined according to the lime fixation point concept (Hilt & Davison 1960). Hilt & Davidson (1960) measured the unconfined compressive strength of specimens containing 0, 1, 2, 3, 4, 5, 6, 8 and 12% lime by dry weight of soil. Based on their results, the unconfined compressive strength of the soil-lime mixtures increased when the plastic limit remained constant with further lime addition.

Specimens were statically compacted according to AASHTO T 307 with a relative compaction equal to 95% of the standard Proctor maximum dry density and optimum water content. Immediately after compaction, ESR specimens were subjected to testing. Specimens containing fly ash were compacted 2 hours after the addition of fly ash and were then allowed to cure for seven days at about 22 degrees Celsius before being tested. Specimens were subjected to unconfined compression tests with a mean effective stress of 100 kPa in order to assess whether

the fly ash content induced pozzolanic reactions. Conventional external transducers were used during consolidated undrained triaxial compression in order evaluate large strain stiffness, while bender elements were used to evaluate small strain stiffness.

The results of this study suggested that the addition of fly ash and the curing time of 7 days promoted the development of pozzolanic reactions in the ESR-fly ash mixtures. Also, the improvements in strength caused by the addition of the off-specification fly ash were similar to those of the Class C fly ash. The large strain stiffness of the ESR-fly ash mixtures was equal to or higher than the expansive soil alone. The small strain stiffness of the ESR-fly ash mixtures was higher than the ESR mixtures and the expansive soil alone.

CHAPTER 3. CONCEPTUAL FRAMEWORK

3.1 Large & Small Strain Stiffness

Young's or elastic Modulus (E) is defined as the ratio of axial stress (σ_a) to axial strain (ε_a), and it is used to represent the stiffness of soil elements subjected to axial loading according to:

$$E = \frac{\sigma_a}{\varepsilon_a} \qquad \text{Equation 3.1}$$

Muir Wood (2009) explains Young's Modulus by using the example of a piece of wire. Imagine a wire fixed to a ceiling, and loaded with weights. The applied load divided by the cross-sectional area of the wire defines the axial stress applied to the wire. Axial strain is determined by the change in length (Δl) divided by the original length (l) of wire. As l increases, the radius (r) of the wire decreases by certain amount (Δr), which provides the measurement of another elastic property, the Poisson's ratio (v) of the material, which is defied as the ratio of radial to axial strain:

$$v = -\frac{\Delta r/r}{\Delta l/l} = -\frac{\varepsilon_r}{\varepsilon_a} \qquad \text{Equation 3.2}$$

were ε_r is defined as the radial strain. The negative sign is needed because the radial strain will be compressive if the axial strain is tensile and vice versa (Muir Wood 2009).

Young's Modulus for soils cannot be determined in the same way Young's Modulus is determined for wire. This is because soil elements are typically compressed instead of pulled. Sand can be compressed in various ways, such as in one-dimensional confined compression, or in one-dimensional unconfined compression (may be impossible, if uncemented). Axial and lateral stresses are applied during confined compression. However, only axial forces are at work in unconfined compression. "The stiffness in one-dimensional confined compression (E_0) is

shown below:

$$E_o = E\frac{(1-v)}{(1-2v)(1+v)} \quad \text{Equation 3.3}$$

and will be greater than the Young's modulus, (E), which is the stiffness for one-dimensional unconfined compression" (Muir Wood 2009). If Poisson's ratio is equal to 0.5, then E_o is infinite. "The material cannot expand laterally and therefore cannot compress axially either" (Muir Wood 2009). Therefore, large strain stiffness is observed as E.

When compressing soil, the compression is irreversible and not linear. Consequently, soil stiffness is measured as a function of strain. Young's modulus (E), tangent stiffness (E_t) and secant stiffness (E_s), maybe determined during triaxial testing from external displacement transducers for axial strains larger than 0.1% (Atkinson 2000). Tangent stiffness is determined from the axial strain (e_a) vs. deviatoric stress (q) curve as the slope of any line tangent to any point on that curve. Muir Wood (2004) defines tangent stiffness as:

$$E_t = \frac{\delta\tau}{\delta\gamma} \quad \text{Equation 3.4}$$

where $\delta\tau$ and $\delta\gamma$ are defined as shear stress and the shear strain increments. Secant stiffness is the slope of the secant line from the origin through the same point on the e_a vs. q curve. Muir Wood (2004) defines secant stiffness as:

$$E_s = \frac{\tau}{\gamma} \quad \text{Equation 3.5}$$

where τ and γ are defined as shear stress and shear strain. Soil stiffness can also be expressed in terms of the shear modulus (G), which can be determined from undrained triaxial compression tests from the e_a vs. q curve or from Young's modulus and Poisson's ratio (v equals 0.5, for incompressible materials). The equation for shear modulus is:

$$G = \frac{\delta q}{3\delta\varepsilon_a} = \frac{E}{2(1+v)}$$ Equation 3.6

where δq and $\delta\varepsilon_a$ are the deviatoric stress and axial strain increments, and v is the Poisson's ratio of the material. Equations 3.4, 3.5, and 3.6 assume an elastic treatment for the incremental response of the materials even though their overall stress-strain response may be far from linearly elastic. Figure 3.1 is an illustration of stiffness parameters for non-linear soil or defines basic strength and stiffness parameters for a triaxial test. Note that E_o is Figure 3.1 refers to the stiffness at very small strains near the start of loading

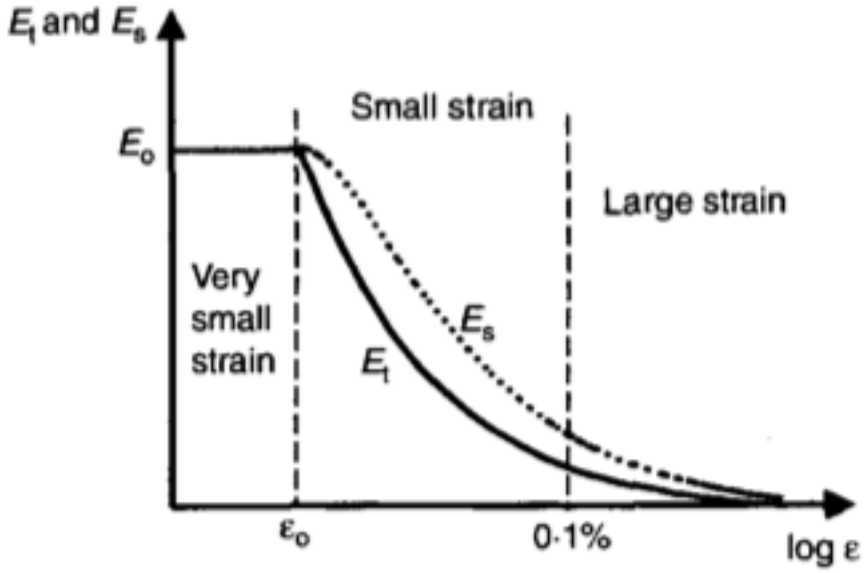

Figure 3.1: Stiffness parameters for non-linear soil (Atkinson 2000)

In general, axial strains greater than 0.1% are considered large strains, and axial strains less than 0.1% are considered small strains (Atkinson 2000). External displacement transducers are used for axial strains larger than 0.1% (Atkinson 2000). Axial strains between 0.001 and 0.1% require the use of local displacement transducers. Alternatively, bender element tests allow measurement of shear wave velocity (V_s), which can be used to determine the maximum shear

modulus for small axial strains between 0.0001 and 0.001%. Equation 3.7 shows the equation for shear modulus using shear wave velocity

$$G = \rho V_s^2 \qquad \text{Equation 3.7}$$

where *r* is the total density of the material. Very small strain stiffness of a soil refers to the range of strain where linear elastic behavior is observed. Figure 3.2 is a representation of soil shear stiffness as a function of shear strain for laboratory tests and structures.

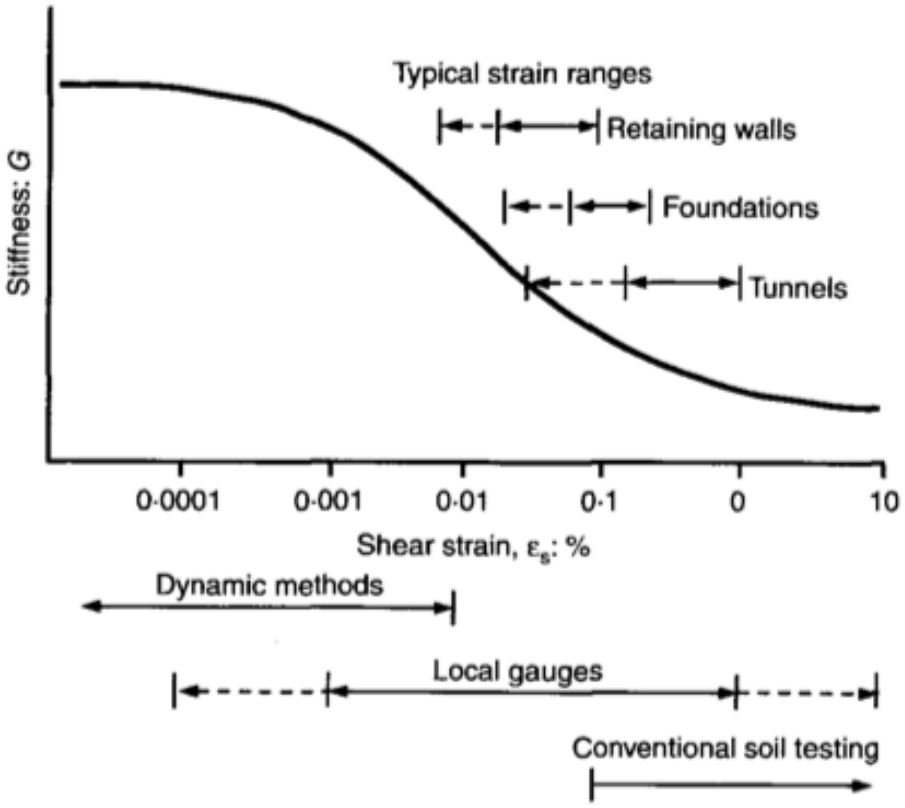

Figure 3.2: Shear Strain Degradation curve (Atkinson 2000)

3.2 Resilient Modulus

Young's modulus is often used in the design of a pavement structure. However, this may not constitute a viable approach because Young's modulus, as well as all the other stiffness parameters listed in section 3.1, might be typically determined during monotonic (static) triaxial tests. Soils in pavement structures undergo cyclic loads, and therefore a resilient modulus (M_r)

has been proposed instead for the pavement design in this study because the M_r only represents the elastic response in cyclic tests and ignores the permanent deformation. The resilient modulus is determined from a specific type of cyclic triaxial test, and is defined as the ratio of the amplitude of the repeated axial stress increment ($\Delta\sigma_a$) to the amplitude of the resultant recoverable axial strain increment ($\Delta\varepsilon_a$) (AASHTO T 307-99 2003) as per:

$$M_r = \frac{\Delta\sigma_a}{\Delta\varepsilon_a} \qquad \text{Equation 3.8}$$

3.3 Computer Software

3.3.1 Computer Software Notation

In this study, Weslea for Windows 3.0 (Timm et al. 1999) is the software used for the computer simulations. Weslea for Windows is a program designed to calculate and analyze the response of pavement structures to applied tire loads. Stress (*s*), strain (*e*), and displacement (*u*) are the three terms that define pavement response in the software. Stresses computed in Weslea are due to external loads only. Stress is the ratio of an applied load (*P*) over a unit area (*A*).

$$\sigma = \frac{P}{A} \qquad \text{Equation 3.9}$$

Strain is the ratio of the change in a certain dimension (Δz) over the original dimension (z).

$$\varepsilon = \frac{\Delta z}{z} \qquad \text{Equation 3.10}$$

The sign convention for stress and strain is negative for tension, and positive for compression. An illustration of the positive stress condition on an element, and positive displacement is given in Figure 3.3. The x, y, z coordinate system used in the Weslea program is displayed in Figure 3.4.

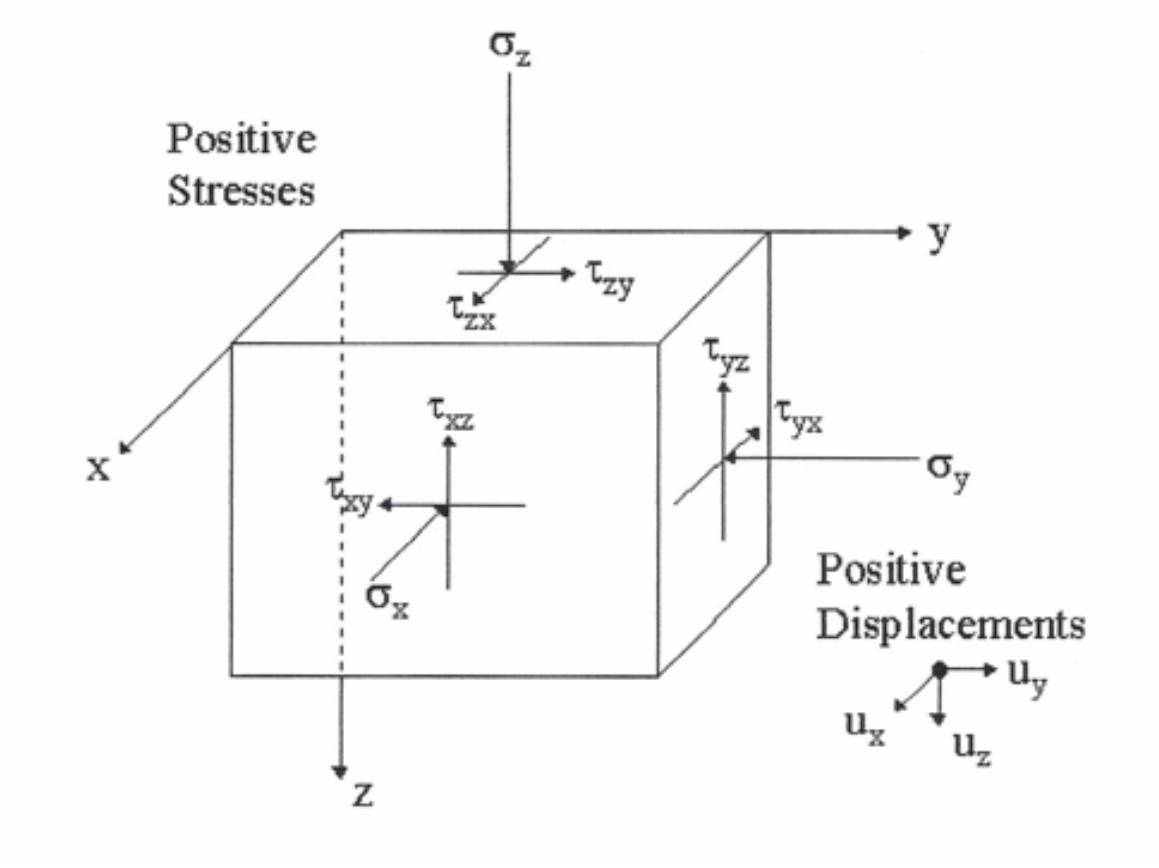

Figure 3.3: Weslea Sign Convention (Timm et al. 1999)

Where u_x, u_y, and u_z, are displacement in the x, y, and z direction. Shear stresses are represented by τ_{xy}, τ_{xz}, τ_{zx}, τ_{zy}, τ_{yz}, and τ_{yx}, while the normal stresses are represented by σ_x, σ_y, and σ_z.

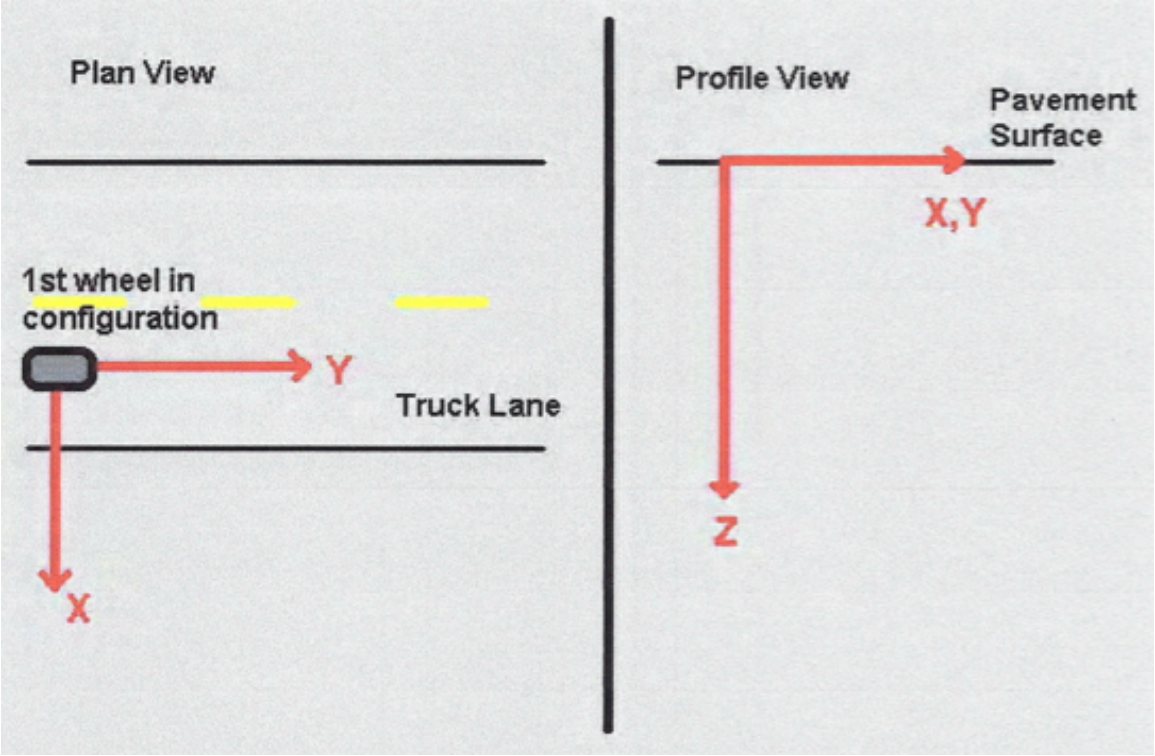

Figure 3.4: Weslea Coordinate System (Timm et al. 1999)

The x and y directions represent the horizontal plane, and the z directions represent vertical planes. The x direction is perpendicular to the flow of traffic, and the y direction is parallel to the flow of traffic.

3.3.2 Software Input Parameters

Weslea software requires three main inputs, which are related to structure characteristics, load conditions, and evaluation at critical locations.

3.3.2.1 Structural Input

The number of layers is selected in the structural input as well as the material type, elastic modulus, Poisson's ratio, layer thickness, and slip condition of each layer. The maximum

number of layers that can be selected is five. However, for this research, only three layers were selected and used in simulations. The first layer is referred to as the asphalt concrete layer. The main purposes of the asphalt concrete layer are:

- To provide a smooth, skid-resistant riding surface;
- To resist distortion under traffic; and
- To provide a waterproof surface in order to protect the layers beneath.

The second layer directly beneath the asphalt concrete layer is referred to as the base layer. The purpose of the base layer is to prevent the asphalt concrete from becoming damaged by local expansive soil subgrade. The third and last layer is known as the subgrade and is located directly beneath the base layer. This layer is the local soil that already exists in the ground (Huang 2004).

Weslea provides six material types, which are asphalt concrete (AC), portland cement concrete (PCC), granular base (GB), soil, rock and other.

Weslea relates the elastic modulus as the stiffness of the material. Young's Modulus (E) is often used as the modulus for soils in pavement design software such as Weslea, instead of the Resilient modulus (M_r). However, for this research, M_r was used to characterize the moduli of the materials.

As discussed previously, Poisson's ratio is a material parameter that describes how the material deforms. Poisson's ratio was previously defined in Equation 3.2, however Weslea for Windows uses the equation below to define to Poisson's ratio.

$$v = -\frac{\varepsilon_{lat}}{\varepsilon_{long}} \qquad \text{Equation 3.11}$$

where ε_{lat} is the lateral strain and ε_{long} is the longitudinal strain.

Weslea allows the user to select the thickness of each layer. However, the subgrade layer is always set to be a continuous layer by default.

Two options are provided for the slip condition, which are full adhesion (no slip) and no adhesion (full slip). When full adhesion is selected it means that there is no relative motion between the pavement layers, and when no adhesion is selected it means that there is relative motion between the layers.

3.3.2.2 Load Conditions

Load conditions is the second main input, and this is where the load configuration, number of load applications, load magnitude, tire pressure, and tire location are specified. Weslea only evaluates half of an axle due to the symmetry of most axles, which can be seen in Figure 3.5.

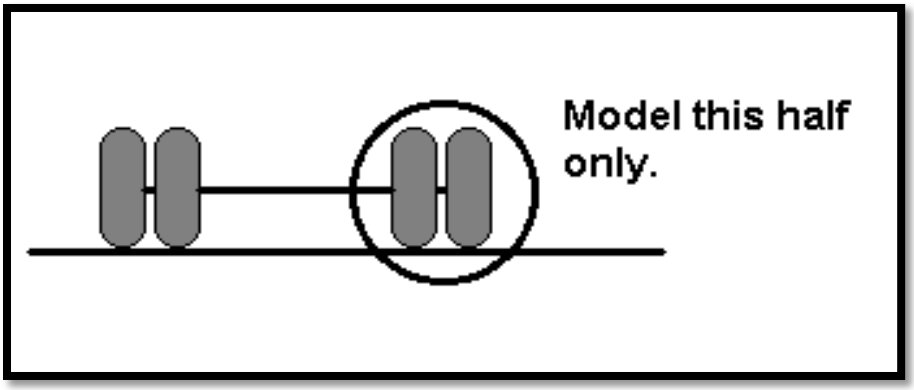

Figure 3.5: Load Analyses in Weslea (Timm et al. 1999)

Weslea has five load configurations to select from, which are single, tandem, tridem, steer, and other. An illustration of each load configuration is displayed in Figures 3.6, 3.7, 3.8, and 3.9. If the option "other" is chosen, then the load information has to be entered manually.

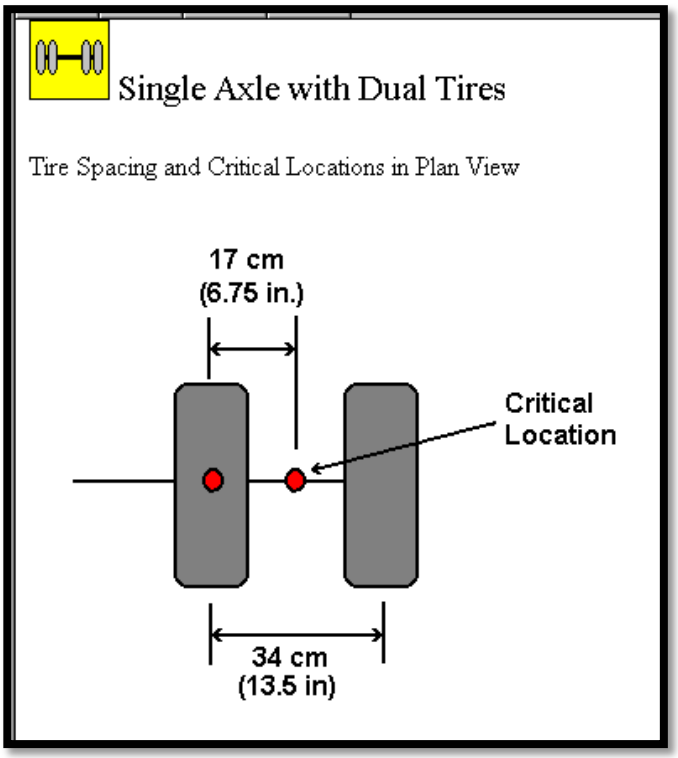

Figure 3.6: Single Load Configuration (Timm et al. 1999)

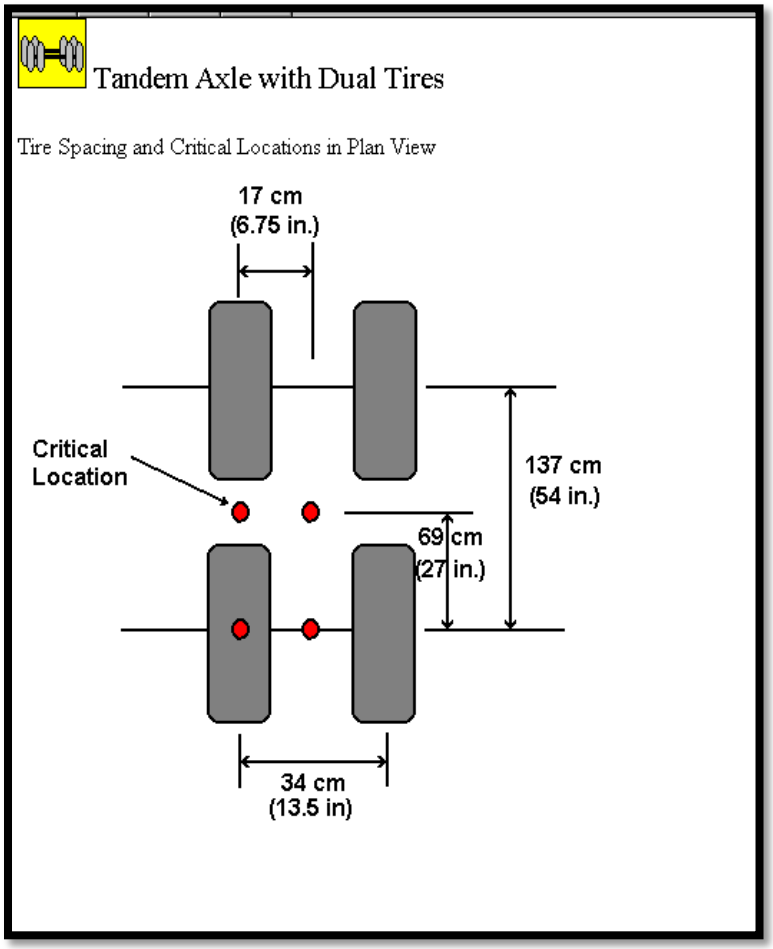

Figure 3.7: Tandem Load Configuration (Timm et al. 1999)

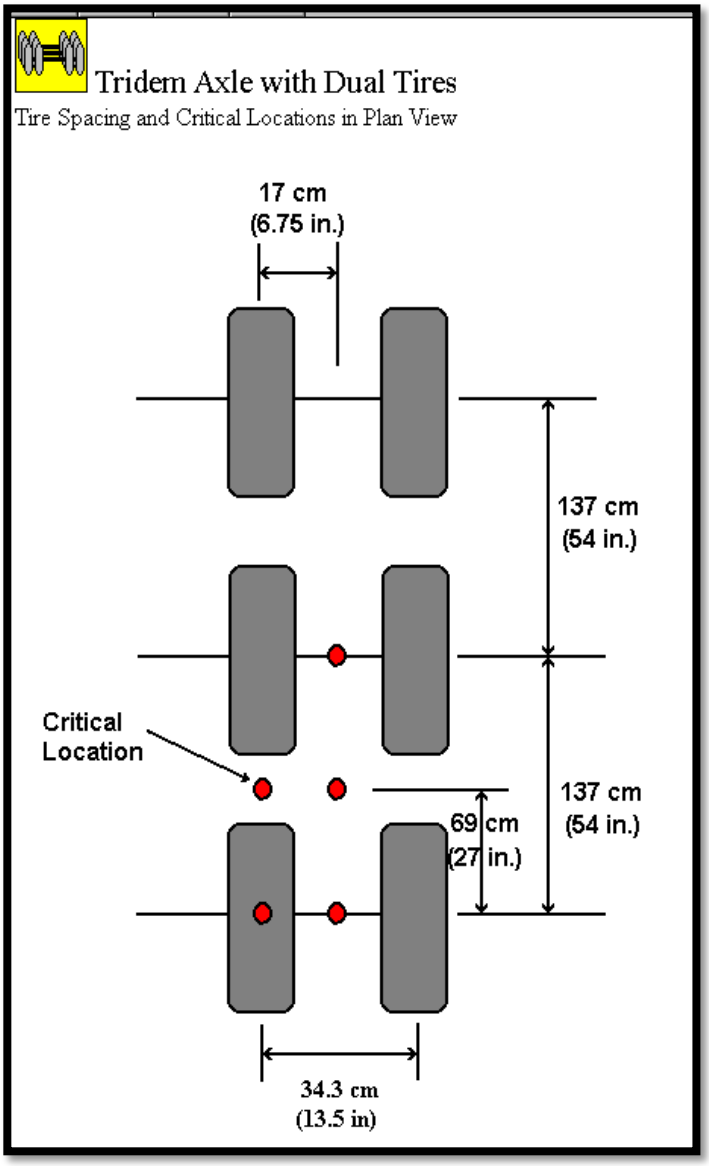

Figure 3.8: Tridem Load Configuration (Timm et al. 1999)

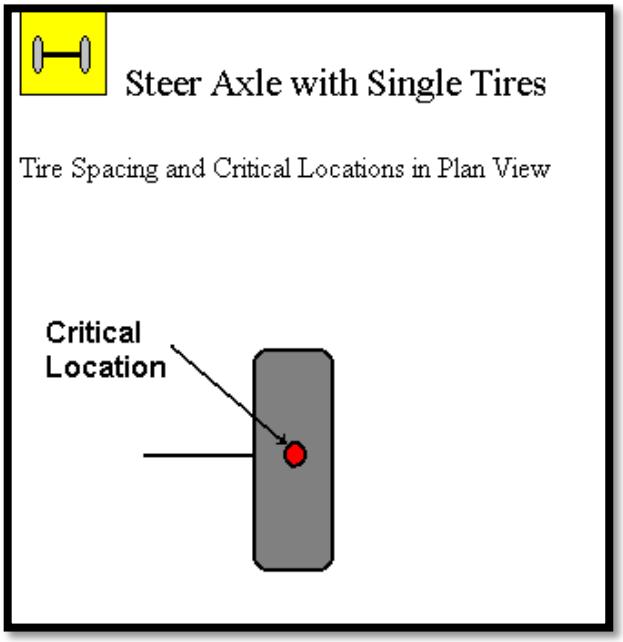

Figure 3.9: Steer Load Configuration (Timm et al. 1999)

"The total number of load applications refers to the total number of repeated applications of the specified wheel configuration that the pavement will experience. This value is used in Miner's Hypothesis to estimate damage" (Timm et al. 1999). The load magnitude is the load imposed on the pavement by each tire of the specified wheel configuration. Tire pressure is the tire inflation pressure, and it is used to calculate the contact area between the tire and road. Weslea assumes the area to be circular, and uses Equation 3.12 to calculate the contact area as:

$$Contact\ Area = \frac{Tire\ Load}{Tire\ Pressure} \qquad \text{Equation 3.12}$$

3.3.2.3 Evaluation of Critical Locations

Evaluation is the third main input, and this is where the critical locations that are to be evaluated in the pavement are specified. Weslea determines the stress, strain, and deflection at these locations. There is an option to use standard (default) locations, or to choose locations manually.

Up to 50 locations can be selected for analyses. Default values are located at the bottom of the first layer and at the top of the subgrade layer. A diagram of the critical locations is provided in Figure 3.10. Weslea uses the horizontal tensile strain (ε_t) at the bottom of the first layer to determine fatigue because it is the highest negative strain value in the x and y directions. However, this value is entered as a positive number into the fatigue equation. Weslea uses the vertical compressive strain (ε_v) at the top of the subgrade to determine rutting because this value is the highest positive value in the z direction. The x and y locations are usually specified directly beneath tires and at the midpoint between tires. These locations will generally yield the greatest strain and experience the most damage. The critical locations are selected by default if a standard load configuration is chosen. However, the critical locations have to be specified by the user if a non-standard configuration is selected.

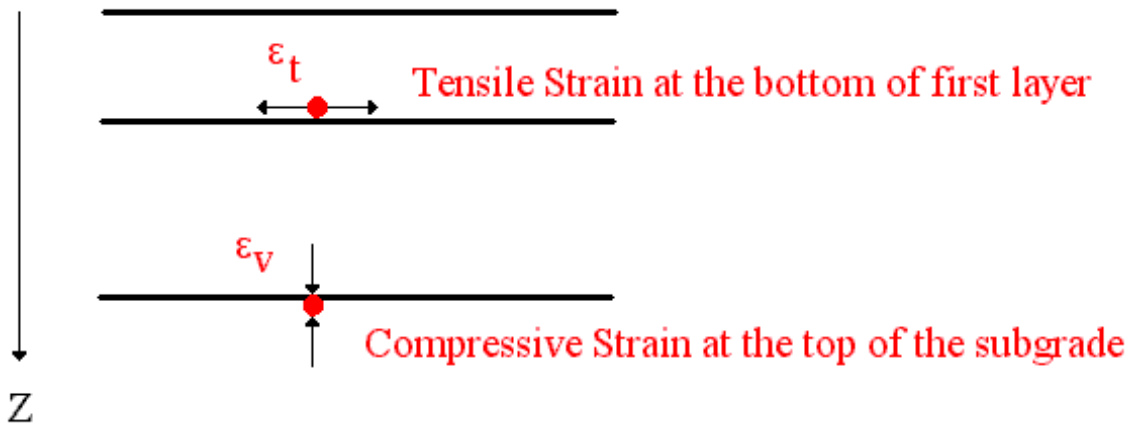

Figure 3.10: Weslea Critical Locations (Timm et al. 1999)

Once all the input information is entered, the output dialog box provides the Weslea mechanistic analysis, which consists of the pavement response data such as the fatigue life, rutting life, and

damage ratio (which will be discussed further in Section 3.3.3) for the selected critical locations. The relative damage ratio for fatigue and rutting is also provided.

3.3.3 Software Output Parameters

3.3.3.1 Fatigue

Fatigue refers to cracks that form in the pavement due to repeated tensile stresses and strains induced at the bottom of the first (or topmost) pavement layer. Weslea used Mn/ROAD fatigue crack data to modify an equation (Thompson 1987) developed at the University of Illinois to predict the fatigue life (N_f), meaning the number of repeated loads until fatigue failure. The equation for fatigue life is:

$$N_f = 2.83x10^{-6}(\frac{10^6}{\varepsilon_t})^{3.148} \quad \text{Equation 3.13}$$

where e_t is the maximum horizontal tensile strain (in microstrain) at the bottom of the first layer caused by one pass of current wheel configuration (Timm et al. 1999).

3.3.3.2 Rutting

Rutting predictions in Weslea software are related to the applied stresses in the subgrade layer. Weslea used Mn/ROAD pavement performance data to develop an equation that predicts rutting of 20 mm. The Mn/ROAD Rutting Equation is:

$$N_f = 1.0x10^{16}\left(\frac{1}{\varepsilon_v}\right)^{3.87} \quad \text{Equation 3.14}$$

where :N_f is the number of applied repeated loads under current structural conditions before rutting failure will occur, and e_v is the maximum vertical compressive strain (in microstrain) at the top of the subgrade caused by one pass of current wheel configuration (Timm et al. 1999).

3.3.3.3 Miner's Hypothesis

Miner's Hypothesis is the summation of the applied number of loads over the allowable number of loads, and is used to estimate cumulative pavement damage (Timm et al. 1999). Miner's Hypothesis is expressed as:

$$D = \sum \frac{n_i}{N_{fi}} \qquad \text{Equation 3.15}$$

where D is the accumulated damage, n_i is the number of applied repeated load applications in condition i, and N_{fi} is the number of allowable repetitions in condition i calculated from fatigue or rutting performance equations. Condition i refers to the combination of material properties, axle type, and axle load that cause a particular strain level. If the number of applied loads exceeds the number of allowable loads, then failure will occur, which means that D must be greater than one.

CHAPTER 4. RESEARCH METHODS

4.1 Experimental Framework

4.1.1 Materials

4.1.1.1 Origin and Location

The expansive soil tested in this study belongs to the Pierre shale formation found in the Front Range of Northern Colorado, and was obtained at the Colorado State University (CSU) expansive soil test site. The CSU test site is located at the Engineering Research Center of Colorado State University. Figure 4.1 shows a detailed diagram of the sampling site. The scrap tire rubber (STR) used in this study was manufactured by Caliber Recycled Products Inc, from Commerce City, Colorado. The off-specification fly ash tested in this study was produced by Rawhide Energy Station, which is located north of Fort Collins, Colorado. Hereafter, the Rawhide Energy Station fly ash will be referred to as R-fly ash.

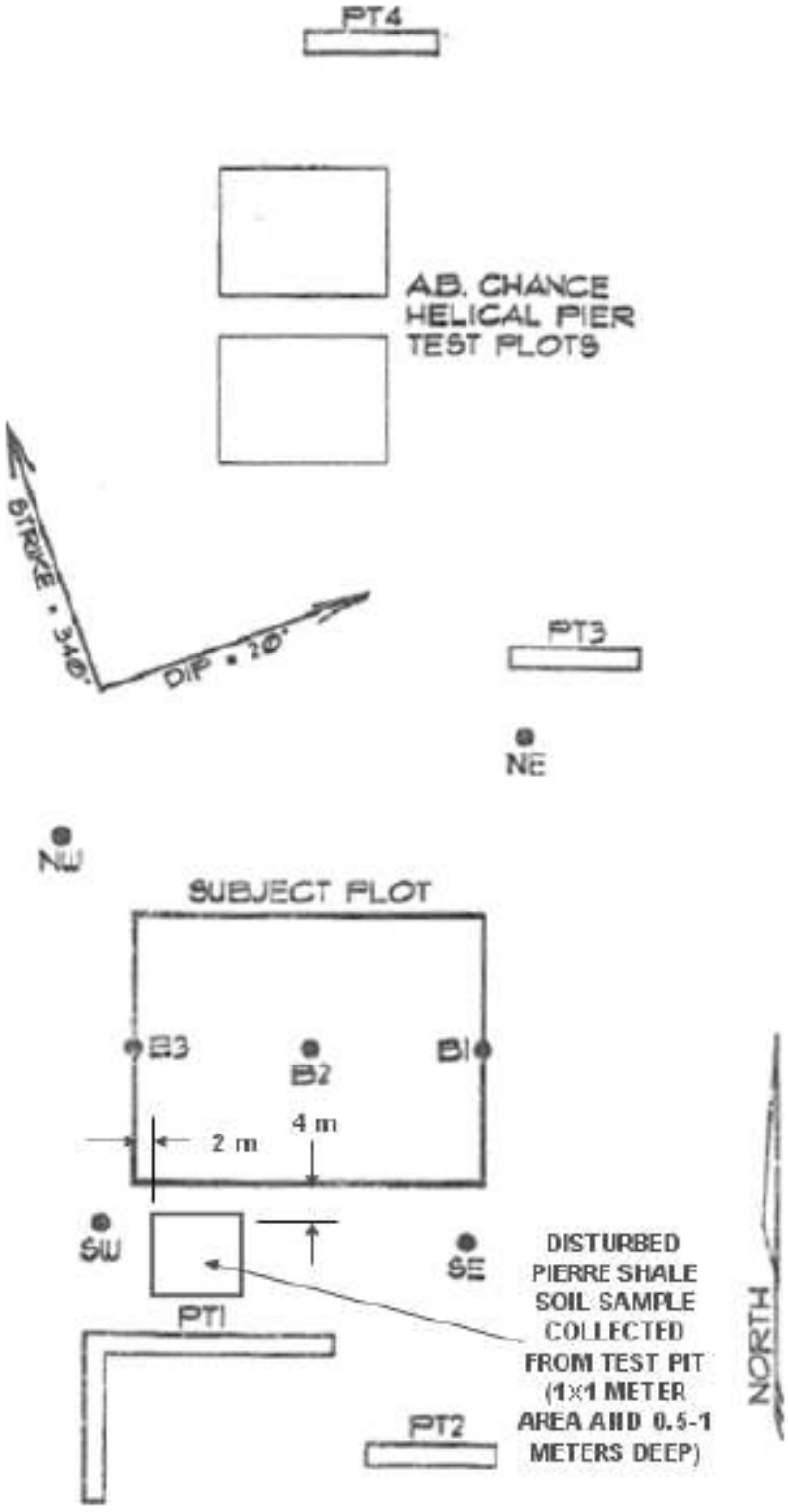

Figure 4.1: Plan View of the Sampling Location (Dunham-Friel 2009, Modified after Abshire 2002)

4.1.1.2 Particle Size Distribution

Figure 4.2 displays the particle size distribution (PSD) of the expansive soil, STR and R-fly ash materials used in the present study, which are the same materials tested by Dunham-Friel (2009) and Wiechert (2011). The PSDs of the expansive soil and STR shown in Fig. 4.2 were originally determined by Dunham-Friel (2009). The PSD of the R-fly ash presented in Fig. 4.2 was determined originally by Wiechert (2011). A comparison of the PSDs of the expansive soil and that of the STR shows that the expansive soil is nonuniform and well-graded, while the STR is uniform and poorly-graded. Based on Figure 4.2, the STR has a maximum nominal particle size of 6.7 mm.

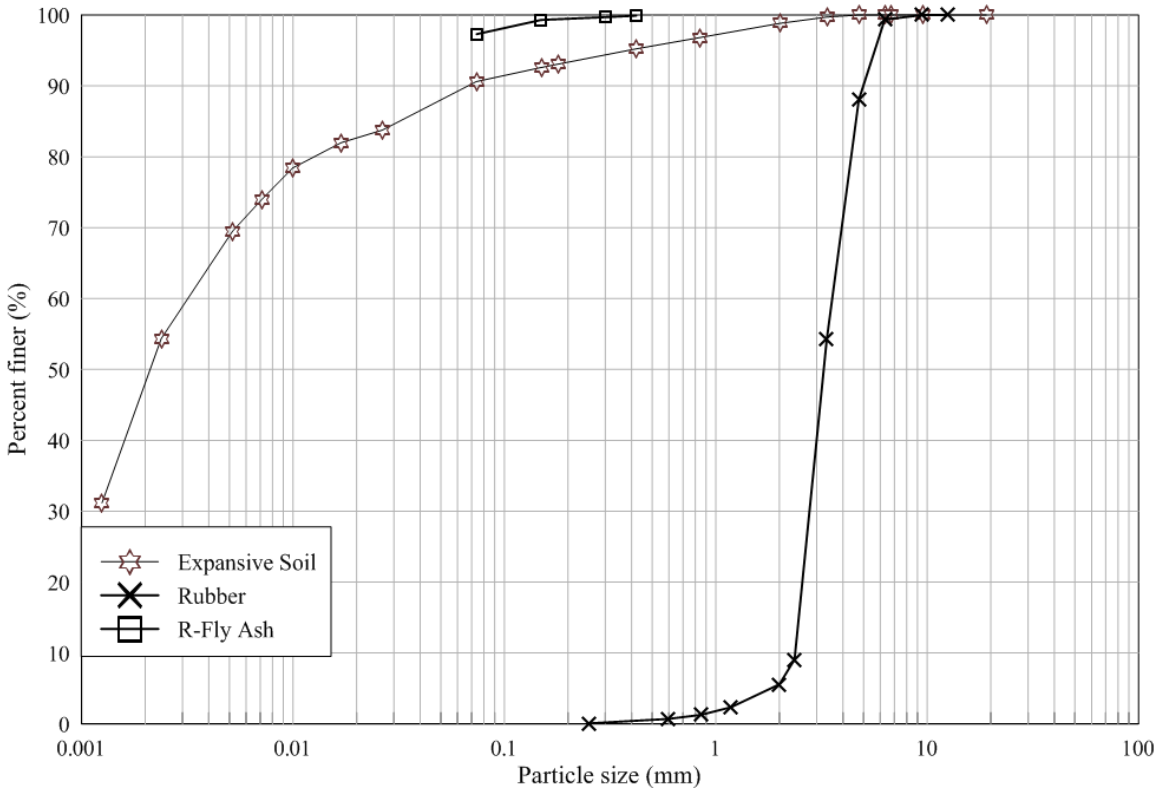

Figure 4.2: Particle Size Distributions of Expansive Soil, Rubber (Dunham-Friel 2009) and R-fly ash (Wiechert 2011)

4.1.1.3 Index Properties

Table 4.1 displays the Atterberg limits determined according to ASTM D 4318 (Wiechert 2011), and the specific gravity (G_s), determined according to ASTM D 422 of the expansive soil (Wiechert 2011). Based on the Unified Soil Classification System, the expansive soil is an inorganic clay of high plasticity (CH), or a fat clay. The specific gravity of the STR determined according to ASTM D 854 is equal to 1.16 (Dunham-Friel 2009).

Table 4.1: Soil Index Properties (Wiechert 2011)

	Liquid Limit, w_L	Plasticity Index, I_P	Specific Gravity, G_s	% Finer No. 4	% Finer No. 200	Uniformity Coefficient, Cu	Coefficient of Curvature, Cc	USCS
Soil	54%	33%	2.72	100	93.1	-	-	CH
STR	-	-	1.16	88	0	1.5	0.91	-
R-fly ash	-	-	2.41	100	98	-	-	-

4.1.1.4 Rawhide Fly Ash

The fly ash has a high sulfur trioxide (SO_3) content and a relatively low amount of pozzolanic materials (<50%). Because of these features, the R-fly ash is an off-specification ash. The chemical composition and specific gravity of the R-fly ash are listed in Table 4.2.

Table 4.2: Chemical Composition and ASTM classification of Rawhide fly ash (Wiechert 2011)

Chemical Constituent	ASTM 618 Requirements	Rawhide Fly Ash
Silicon Dioxide (SiO_2), %		26.6
Aluminum Oxide (Al_2O_3), %		12.8
Iron Oxide (Fe_2O_3),%		5.4
Sum of SiO2, Al2O3, Fe2O3, %	50.0 Min.	44.8
Calcium Oxide (CaO),%		29.7
Magnesium Oxide (MgO), %		5.5
Sulfur Trioxide (SO_3), %	5.0 Max.	12.4
Sodium Oxide (Na_2O), %		1.6
Potassium Oxide (K_2O), %		0.4
Loss on Ignition, %	6.0 Max.	2.5
ASTM Classification	Class C	Off-Spec

4.1.1.4.1 Scanning Electron Microscope

A JSM-6500F Field Emission Scanning Electron Microscope was used by Wiechert (2011) to take scanning electron microscope (SEM) photographs of the R-fly ash, and can be viewed in Figure 4.3. The photos were taken by the Department of Chemistry in the Central Instruments Facility at CSU. The micro-fabric (approximately 10 to 50 mm) and the mini-fabric (approximately 100 to 500 mm) can be observed in the SEM photos d, e, and f in Figure 4.3.

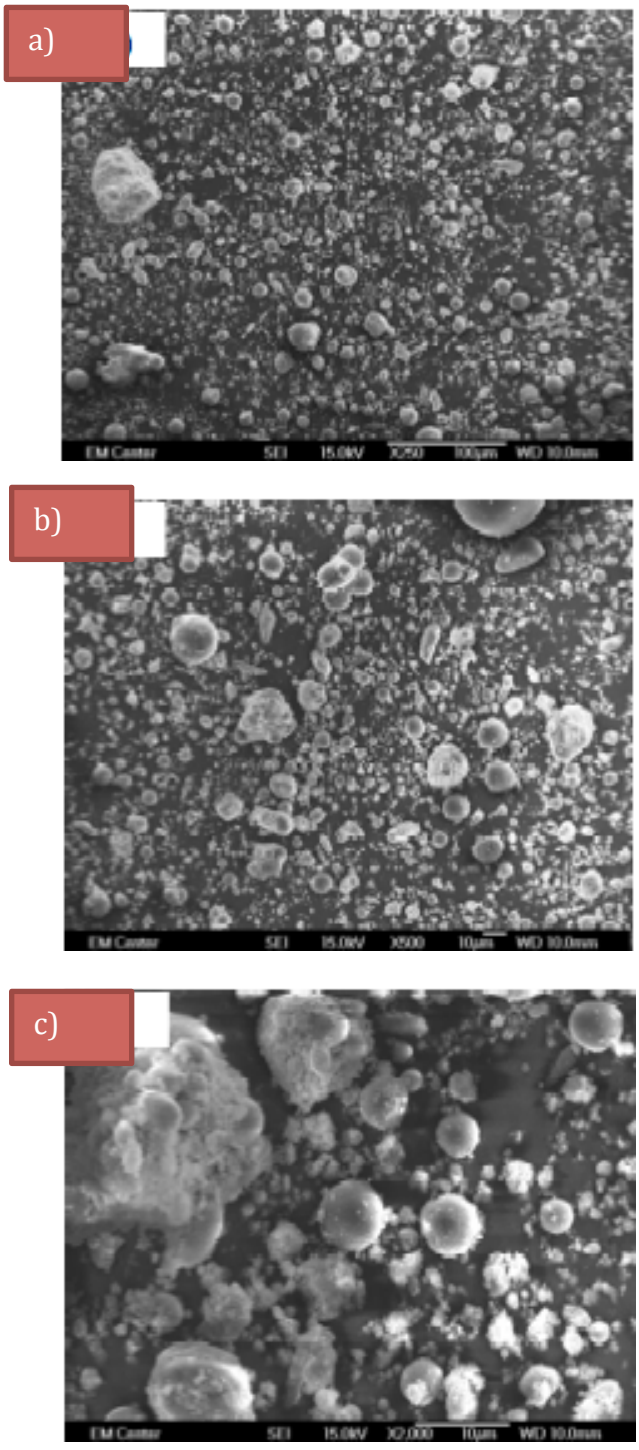

Figure 4.3: SEM photographs of R-fly ash: (a) x250, (b) x500, (c) 2000 (Wiechert 2011)

4.1.1.5 Compaction Parameters

The standard proctor curves and data points for the expansive soil, ESR mixture, and ESR-R mixture are displayed in Figure 4.4. Figure 4.4 shows that the maximum dry density and the optimum water content decrease with the addition of STR, which is due to the lower specific gravity of the STR as well as lower compaction efficiency during ESR compaction. The addition of R-fly ash slightly decreases the maximum dry density and the optimum water content compared to the expansive soil alone and the ESR mixtures. The Standard Proctor compaction parameters in (determined according to ASTM D 698) for the expansive soil, ESR mixture, and ESR-FA mixture are listed in Table 4.3. The ESR-FA mixture used in this study is listed as ESR-R in Table 4.3.

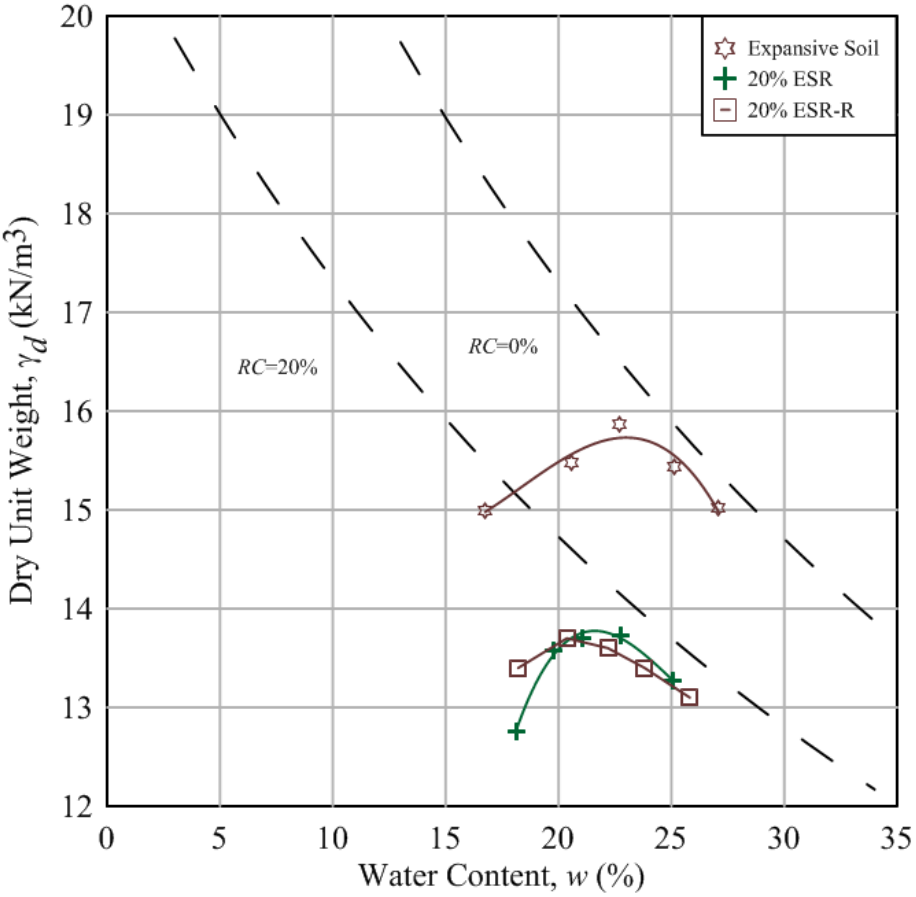

Figure 4.4: Variation of dry unit weight with water content using the standard compaction effort (ASTM D 698) for materials tested (Wiechert, 2011)

Table 4.3: Compaction Parameters for expansive soil, ESR, and ESR-fly ash mixture (Wiechert, 2011)

Material	Standard Proctor (ASTM D 698)	
	Maximum Dry Unit Weight, γ_d	Optimum Water Content, w_{opt}
	(kN/m^3)	(%)
Expansive Soil	15.7	23.0
ESR	13.8	21.6
ESR-R	13.7	20.9

4.1.2 Mixture Design

Three materials were tested in this study, which were expansive soil (ES), expansive soil-rubber (ESR) mixture, and expansive soil-rubber stabilized with off-specification fly ash (ESR-FA) mixtures. The rubber content (*RC*) parameter used to determine the amount of rubber in the ESR mixtures is defined as the ratio of the dry mass of rubber (m_R) to the total dry mass of solids:

$$RC(\%) = \frac{m_R}{m_R + m_s} * 100 \qquad \text{Equation 4.1}$$

where m_s is the total dry mass of the soil. The ESR mixture consisted of expansive soil with an *RC* of 20 %.

The lime fixation point method was used by Wiechert (2011) to determine the fly ash content (*FAC*) to be added to the ESR mixtures in order to develop pozzolanic reactions with the soil (Hilt and Davidson 1960). Hilt & Davidson (1960) measured the unconfined compressive strength of specimens containing 0, 1, 2, 3, 4, 5, 6, 8 and 12% lime by dry weight of soil. Based on their results, the unconfined compressive strength of the soil-lime mixtures increased when the plastic limit remained constant with further lime addition.

Wiechert (2011) hypothesized that the ESR-FA mixtures would develop similar plasticity change characteristics as a result of additions of fly ash. Wiechert (2011) determined the plasticity characteristics of soil-fly ash blends by using Atterberg limit tests in accordance with ASTM D 4318. The *FAC* is defined as:

$$FAC(\%) = \frac{M_{FA}}{M_S + M_{FA}} * 100 \qquad \text{Equation 4.2}$$

where M_s is the dry mass of the soil, and M_{FA} is the dry mass of fly ash. Wiechert (2011) concluded that an *FAC* of 14% for was appropriate for ESR-FA mixtures with R-fly ash. The

ESR-FA mixture consisted of expansive soil with an *RC* of 20 % and an *FAC* of 14%. The *RC* for ESR-FA mixtures is further defined as:

$$RC(\%) = \frac{M_R}{M_R + M_S + M_{FA}} \qquad \text{Equation 4.3}$$

4.1.3 Specimen Preparation

4.1.3.1 Expansive Soil Specimen Preparation

The expansive soil was processed though a No. 4 sieve, and then oven dried at 110^{o}C for 24 h in order to obtain a water content equal to 0%. After 24 h, the expansive soil was allowed to cool down and then poured into a plastic bag, and increments of de-ionized water were added through a spray bottle until the optimum water content was obtained. The expansive soil mixture was then sealed in an airtight plastic bag and cured at for 24 h at 21^{0}C to allow the water content to become uniform.

4.1.3.2 ESR Specimen Preparation

The expansive soil and granulated rubber were processed though a No. 4 sieve, and then oven dried (expansive soil was oven dried at 110^{o}C and the STR was oven dried at 60^{o}C) for 24 h. After 24 h, the expansive soil and granulated rubber were allowed to cool down and then were mixed in a plastic bag. Once the expansive soil or ESR mixture had cooled, increments of de-ionized water were added through a spray bottle until the optimum water content was obtained. The ESR mixture was then sealed in an airtight plastic bag and cured for 24 h at 21^{0}C to allow the water content to become uniform.

4.1.3.3 ESR-FA Specimen Preparation

The expansive soil and granulated rubber were processed though a No. 4 sieve, and then oven dried (expansive soil was oven dried at 110^{o}C and the STR was oven dried at 60^{o}C) for 24 h. After 24 h, the expansive soil and granulated rubber were allowed to cool down and then were mixed in a plastic bag. Increments of de-ionized water were added through a spray bottle until the water content was slightly less than the optimum water content. The reason for not adding the full amount of water needed to obtain the optimum water content was so that additional water could be mixed in when the R-fly ash was added, which makes the process of mixing in the R-fly ash easier. The mixture was then sealed in an airtight plastic bag and cured for 22 at h 21^{0}C to allow the water content to become uniform. After this period, the R-fly ash was added to the mixture with the additional amount of water needed to reach optimum water content. The ESR-FA mixture soaked for 1 to 2 h at 21^{0}C before compaction.

4.1.4 Compaction Procedure

All specimens were compacted in accordance with the AASHTO T 307-99 static compaction procedure (AASHTO T 307-99 2003), which eliminates the need for specimen trimming (Holtz and Kovacs 1981). The AASHTO T 307-99 procedure compacts the specimens in five layers using the AASHTO T 307-99 compaction mold displayed in Figure 4.5. The layers were compacted on alternating sides of the center lift using a 100-kN load frame, and were scarified prior to the addition of the next lift.

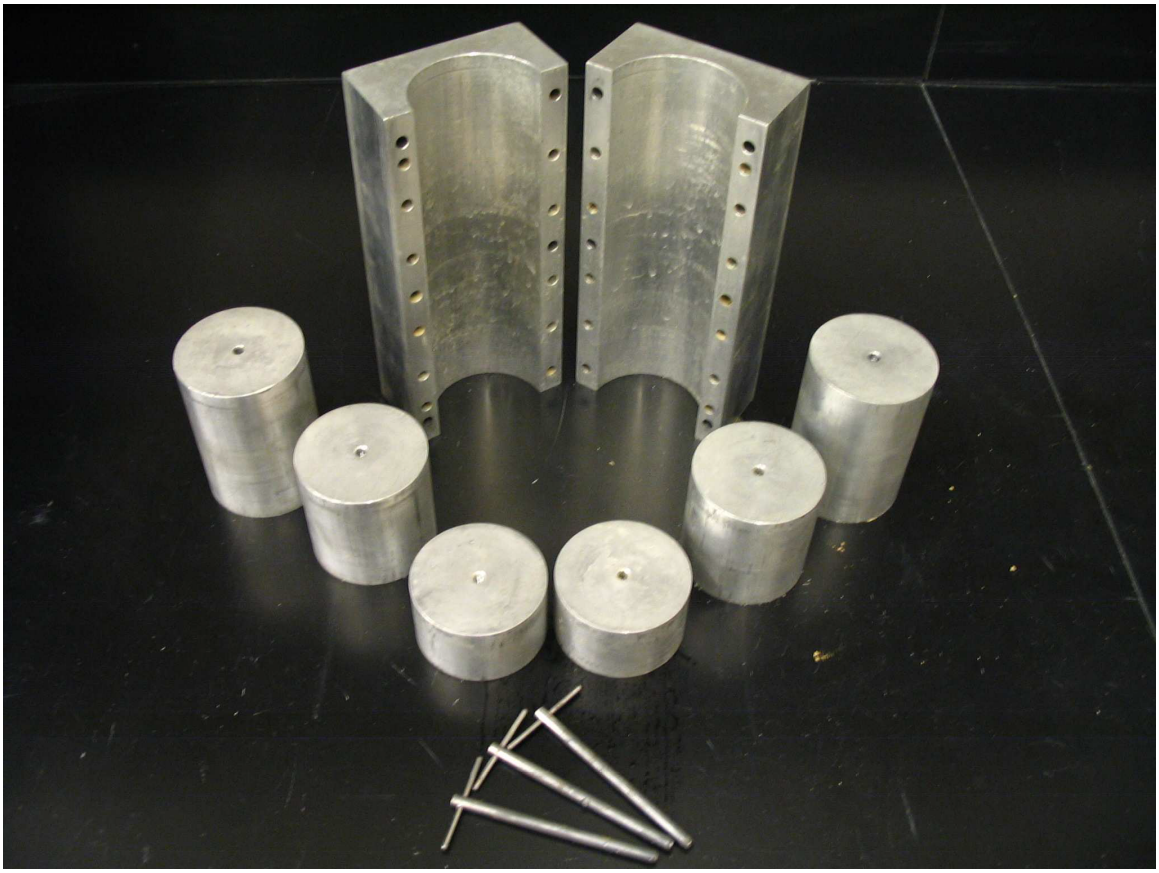

Figure 4.5: AASHTO T 307-99 static compaction mold (Dunham-Friel 2009)

The specimens were compacted within ± 0.5% of a target relative compaction (C_R) equal to 95% of the Standard Proctor maximum dry density (meaning that the relative compaction of the specimens was always between 94.5% to 95.5% of the Standard Proctor maximum dry density). Target relative compaction is defined as the specimen state within the compaction mold when the vertical load applied is equal to zero, which means the specified mass has been compacted to the target specimen volume and no vertical load is further required to keep the target specimen weight. In the case of the ESR and ESR-FA specimen layers, both had to be over -compacted because these specimen layers rebound due to the granulated rubber. This was done through a trial and error process until the compaction mold plugs were perfectly level with the top of the

compaction mold without the application of any vertical load. The average specimen height and diameter were 142 mm and 71 mm, respectively.

Once compacted, the ESR-FA specimens were left in the ASSHTO T 307-99 compaction mold with the compaction mold plugs at the top and bottom of the specimen, and sealed in a plastic bag. ESR-FA specimens were allowed to cure for 7 to 14 days at approximately 22±1.5 ^{0}C before being subjected to testing. On the other hand, expansive soil and ESR specimens were tested immediately after compaction. All specimens were removed from the split mold by sliding the opposing halves of the split mold in opposite directions.

4.1.5 Resilient Modulus Testing

4.1.5.1 Resilient Modulus Equipment

Resilient modulus tests were conducted using a modified dynamic hollow cylinder (DHC) apparatus (Figure 4.6) and a computer-control data acquisition system (CDAS) manufactured by Wykeham Farrance International. UTS009 Unbound Materials Resilient Modulus & Shear Test Software was the software used to process the data. The software was manufactured by IPC Global. The basic differences between the equipment specified in AASHTO T 307 and the equipment used in this study are listed in Table 4.4.

Table 4.4: AASHTO T 307 Equipment versus DHC Equipment

	AASHTO T 307 Specifications	DHC Equipment
Apparatus	Triaxial Pressure Chamber	Dynamic Hollow Cylinder
Measurement of Deformation	Measured with two spring-loaded linear variable differential transducers (LVDT)	Displacement transducer mechanically coupled to the actuator shaft
Confining Fluid	Air	Water
Loading Device	Top loaded, closed loop, electrohydraulic or electropneumatic	Bottom loaded, closed loop, pneumatic actuators

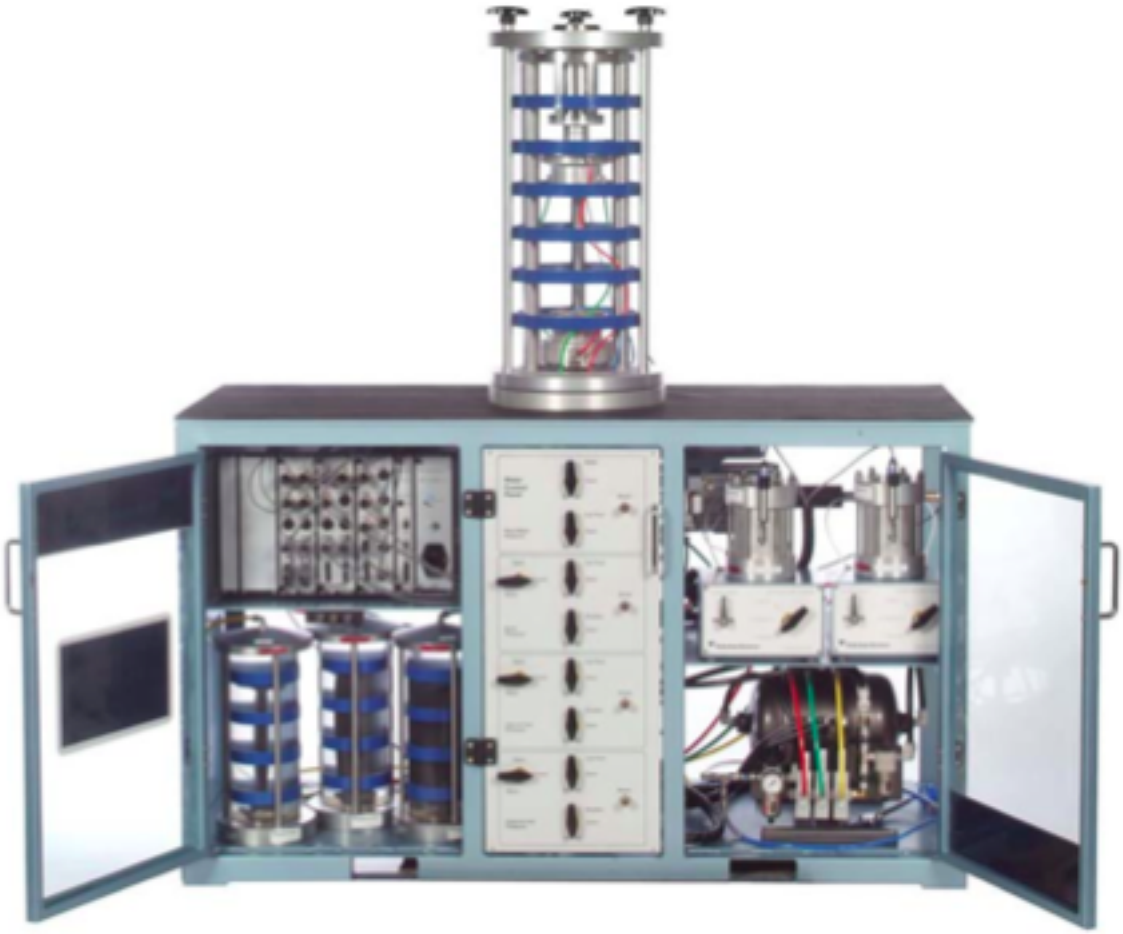

Figure 4.6: Dynamic Hollow Cylinder (Wykeham Farrance 2006)

The triaxial cell in Figure 4.6 has a diameter of 150 mm and can test a specimen with a diameter up to 100 mm. The pneumatic vertical actuator is mounted on the base of the triaxial cell and is fitted with a digital servo valve, which controls the force displacement frequency and wave shape (Wykeham Farrance 2006). The vertical actuator has a range of ± 25 mm and can apply a load of ± 10 kN (Wykeham Farrance 2006). Characteristics of the instruments used can also be seen in Table 4.5.

Table 4.5: Characteristics of Instruments

Digital Instrument	Capacity		Resolution
Vertical (or axial) Actuator Displacement	10 kN	25 mm	
Axial Displacement Transducer	-	25 mm	1.5 micron
Radial Displacement Transducer	-	50 mm	1.5 microm
Outer Cell Pressure Transducer	1000 kPa	-	0.05 kPa

The CDAS provides all critical control, timing and data acquisition functions for the test and the transducers. In other words, the CDAS controls the servo valve to apply the requested loading rate or waveform, cell pressure and backpressure (Wykeham Farrance 2006). The CDAS communicates to the computer through a RS232 C serial interface or high speed USB interface at 10Mb/s. A photo of the CDAS can be seen in Figure 4.7.

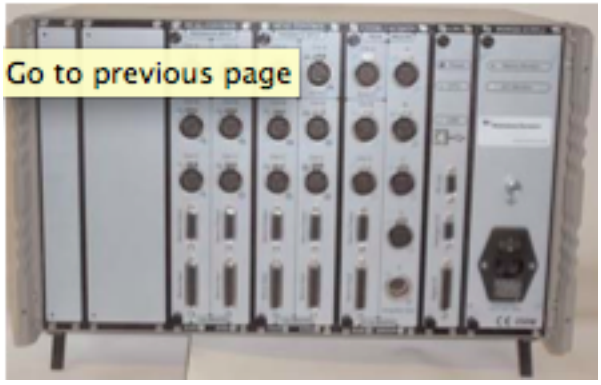

Figure 4.7: Computer Control Data Acquisition System (Wykeham Farrance 2006)

The dynamic hollow cylinder and CDAS are a closed-loop system. In a closed-loop system, the operator enters the control parameters (demand) into the software, which are then sent to the CDAS. The CDAS controls the servo valve to apply the requested loading rate or waveform, cell pressure and backpressure (Wykeham Farrance 2006). The transducers record data (feedback) during the test, which is sent directly to the CDAS and then to the PC where it can be displayed and stored. The CDAS compares the demand to the feedback. The difference between the two signals (error) is used to drive the servo valve to regulate the flow of the hydraulic fluid or air pressure in the direction needed to eliminate the error (Wykeham Farrance 2006). Figure 4.8 represents a closed-loop system.

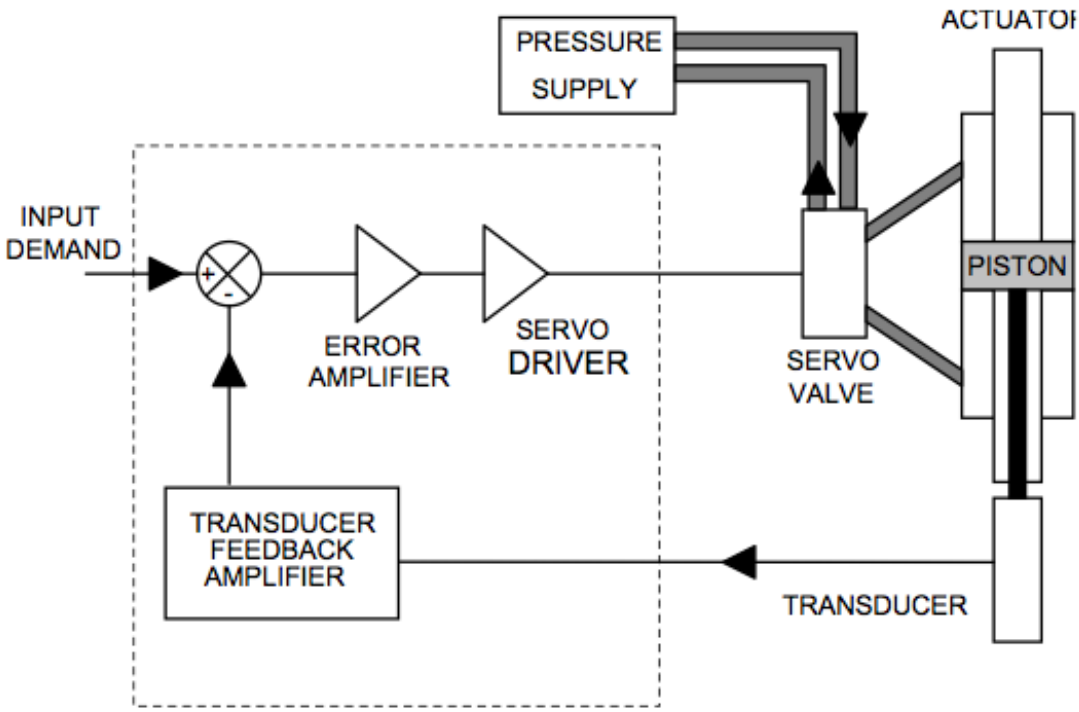

Figure 4.8: Closed Loop System (Wykeham Farrance 2006)

4.1.5.2 Resilient Modulus Test Procedure

The expansive soil, ESR, and ESR-FA specimens were positioned in the triaxial cell immediately after extraction from the mold. Once the specimen was mounted between the base and top pedestal, the triaxial cell took about 30 minutes to fill with de-ionized water. Table 4.6 shows that the ESR-FA specimens that were tested by Wiechert et al. (2011) were flushed, back pressure saturated, and consolidated before shearing. These three extra stages lasted 5 days. In order to keep tests in this study as similar as possible to tests in the study conducted by Wiechert et al. (2011), the ESR-FA specimens were flushed for 2 h and then the valve that allowed the water flow out of the specimen was closed. However, the value that allows water from the tank to flow into the specimen was left open (which applied a head of slightly less than 20 kPa) for 5 days before the resilient modulus testing was conducted.

Table 4.6: Testing schedule for Ethan Wiechert triaxial tests (Wiechert 2011)

Stage of Testing	Duration
Curing in Mold	7 d or 14 d
Flushing	2 d
Back Pressure Saturating	2 d
Consolidating	1 d
Shearing	1 d
Total Approximate Duration	13 d or 20 d

Resilient modulus testing was performed according to ASSHTO T 307-99 standards. Drainage lines were left open during resilient modulus testing in order to simulate drained conditions. The actual resilient modulus test took 1 h to complete. Once the testing was completed, all specimens were oven dried (expansive soil specimens were oven dried at 110°C and ESR and ESR-FA specimens were oven dried at 60°C) for 24 h in order to determine their water content and relative compaction. The ASSHTO T 307-99 control parameters entered into the software are listed in Table 4.7.

Table 4.7: ASSHTO T 307-99 Target Parameters (AASHTO T 307-99 2003)

Sequence No.	Confining Pressure, S_3		Max. Axial Stress S_{max}		Cyclic Stress S_{cyclic}		Constant Stress $0.1S_{max}$		No. of Load Applications
	kPa	psi	kPa	psi	kPa	psi	kPa	psi	
0	41.4	6	27.6	4	24.8	3.6	2.8	.4	500–1000
1	41.4	6	13.8	2	12.4	1.8	1.4	.2	100
2	41.4	6	27.6	4	24.8	3.6	2.8	.4	100
3	41.4	6	41.4	6	37.3	5.4	4.1	.6	100
4	41.4	6	55.2	8	49.7	7.2	5.5	.8	100
5	41.4	6	68.9	10	62.0	9.0	6.9	1.0	100
6	27.6	4	13.8	2	12.4	1.8	1.4	.2	100
7	27.6	4	27.6	4	24.8	3.6	2.8	.4	100
8	27.6	4	41.4	6	37.3	5.4	4.1	.6	100
9	27.6	4	55.2	8	49.7	7.2	5.5	.8	100
10	27.6	4	68.9	10	62.0	9.0	6.9	1.0	100
11	13.8	2	13.8	2	12.4	1.8	1.4	.2	100
12	13.8	2	27.6	4	24.8	3.6	2.8	.4	100
13	13.8	2	41.4	6	37.3	5.4	4.1	.6	100
14	13.8	2	55.2	8	49.7	7.2	5.5	.8	100
15	13.8	2	68.9	10	62.0	9.0	6.9	1.0	100

4.1.6 Poisson's Ratio Testing

4.1.6.1 Poisson's Ratio Equipment

Poisson's ratio tests were conducted using the same dynamic hollow cylinder (DHC) apparatus (Figure 4.6) and computer control data acquisition system (CDAS) described previously, as well as radial and axial transducers manufactured by Wykeham Farrance International. UTS009 Unbound Materials Resilient Modulus & Shear Test Software was the software that processed the data, which was manufactured by IPC Global.

4.1.6.2 Poisson's Ratio Procedure

Expansive soil, ESR, and ESR-FA specimens were subjected to Poisson's ratio testing immediately after extraction from the mold. All specimens were placed between the top and base platen of the DHC, and then an ELE 70 mm membrane was rolled over them. Radial and axial transducers were then glued with superglue to the membrane. The radial transducer was glued to the center of the specimen. The axial transducer came in two pieces. The top piece was glued at a length equal to $1/3^{rd}$ of the height of the specimen from the top of the specimen. The bottom piece was glued $1/3^{rd}$ of the height of the specimen from the bottom of the specimen.

The base platen was then manually raised (using the virtual pendant in the software) in small increments ranging from 0.2 mm to 0.5mm. Each time the base platen was raised, the radial and axial transducer readings were recorded. The triaxial cell was left open during this entire process, meaning that no confining pressure was applied to the specimen. Figure 4.9 shows an expansive soil specimen in the DHC right before the radial and axial transducers were glued onto the membrane.

Figure 4.9: Expansive Soil Specimen in DHC before Radial and Axial Transducers were Glued to Membrane

4.2 Computer Simulations

Weslea for Windows version 3.0 was the software used for the computer simulations. The three main input parameters are structure, load conditions, and evaluation. Default parameters were selected for load conditions and evaluation. This means that the steer load configuration (with a total number of load applications equal to 1000) was used for all the simulations as well as the default critical locations. The first default critical location is located at the bottom of the first layer, and the second default critical location is located at the top of the subgrade layer. Default critical locations can be seen in Figure 3.10.

4.2.1 Combinations

The input parameters required to define the pavement structure to be analyzed are the number of layers, modulus, Poisson's ratio, layer thickness, and slip condition. All simulations were conducted assuming full adhesion (no slip). Simulations for configurations 1.A, 2, and 3 had a total of 3 layers, and simulations for configuration 1.B had a total of 2 layers. The four different pavement structure configurations analyzed are listed below:

1. Asphalt concrete over expansive soil
    1.A. Asphalt concrete over expansive soil base over expansive soil subgrade
    1.B. Asphalt concrete over expansive soil subgrade
2. Asphalt concrete over ESR base over expansive soil subgrade
3. Asphalt concrete over ESR-FA base over expansive soil subgrade

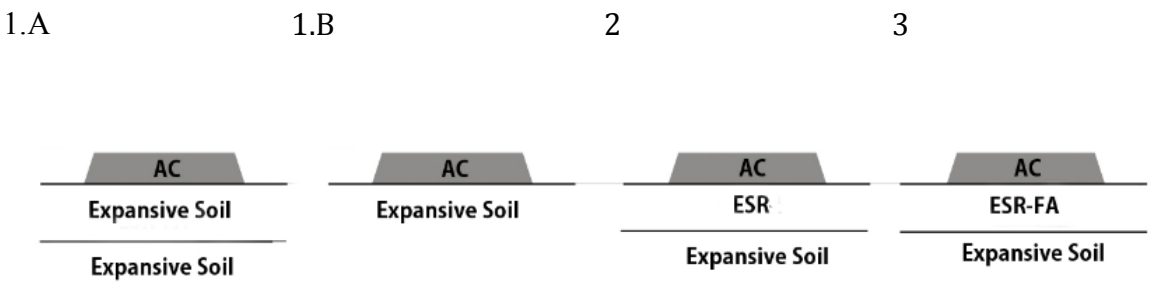

Figure 4.10: Pavement Structure Configurations

The resilient modulus and Poisson's ratio of the expansive soil, ESR, and ESR-FA were defined based on results from the experimental component of this research and were assumed to remain constant for all simulations. The resilient modulus used are discussed in Chapter 5.

For configurations 1.A, 2, and 3 the layer thickness of the first layer (asphalt concrete layer) was always equal to 10.16 cm (4 in), and the third layer (subgrade layer) was always assumed to be infinite. A typical range for the middle (base) layer is 5.08 to 50.8 cm (2 to 20 inches), so four different depths were used in the simulations: 10.16 cm (4 in), 20.32 cm (8 in), 30.48 cm (12 in), and 40.64 cm (16 in). (Huang 2004). In total, 13 scenarios were analyzed. Configuration 1.B had a layer thickness of 10.16 cm

CHAPTER 5. RESULTS

5.1 Experimental Results

5.1.1 Resilient Modulus

Resilient modulus data provided in this section met the following requirements:

1. The water content of expansive soil, ESR, and ESR-FA laboratory-compacted specimens was within +/- 0.5% of the target optimum water content. (e.g. 22.5% < w < 23.5% for the expansive soil specimen);
2. The relative compaction of the laboratory-compacted specimens was within +/- 0.5% of the target relative compaction (e.g. 94.5% < C_R < 95.5% for the expansive soil specimen);
3. The applied contact stress did not vary by more than +/- 0.7 kPa of the target contact stress (e.g. 0.7 kPa < contact stress < 2.1 kPa for sequence 1, all target contact stresses for each sequence are listed in Table 4.7);
4. The ratio of the difference between the actual and the target deviator stresses to the target deviator stress, was not greater than +/- 20% (i.e. see equation below);

$$\frac{q_{mean}-q_{target}}{q_{target}} x\ 100 < 20\% \qquad \text{Equation 5.1}$$

5. All other conditions listed in Table 4.7, which are specified by AASHTO T 307 for each sequence.

The first two requirements were applied to all specimens subjected to testing. Requirements 3 and 4 were applied to all sequences of the resilient modulus test. For example, if sequence 5 of

the AASHTO T 307 resilient modulus procedure did not meet requirements 3 and 4, data for sequence 5 was disregarded. Table 5.1 summarizes the state of all specimens.

Table 5.1: Compaction Parameters of Specimens Tested in the M_r Protocol

Specimen	Test Protocol	Target Compaction Parameters		Actual Compaction Parameters		Water Content Variation	Relative Compaction Variation	Resilient Modulus (range)
		Water Content	Relative Compaction	Water Content	Relative Compaction			
		w	C_R	w	C_R	Δw	ΔC_R	M_r
		%	%	%	%	%	%	MPa
ES 1	M_r	23.0	95.0	22.8	95.2	-0.2	0.2	24 to 51
ESR 1	M_r	21.6	95.0	21.1	95.4	-0.5	0.4	3 to 6
ESR-FA 1	M_r	20.9	95.0	21.1	94.9	0.2	-0.1	5 to 10
ESR-FA 2	M_r	20.9	95.0	21.4	95.3	0.5	0.3	5 to 10
ES 2	v	23.0	95.0	23.0	94.5	0.0	-0.5	NA
ESR 2	v	21.6	95.0	21.5	95.4	-0.1	0.4	NA
ESR-FA 3	v	20.9	95.0	21.1	95.5	0.2	0.5	NA

Figure 5.1 shows the resilient modulus values of the expansive soil, ESR, and ESR-FA specimens tend to decrease with increasing sequence number. This may be primarily due to the fact that the first five sequences (i.e., sequences 1 to 5 as sequence 0 refers to the initial conditioning stage) have the highest confining stress of 41.4 kPa, the second five sequences have a confining stress of 27.6 kPa, and the last five sequences have a confining stress of 13.8 kPa. This decrease in stiffness is also due to stiffness degradation induced on the specimen due to the cumulative cyclic loading induced by the resilient modulus protocol.

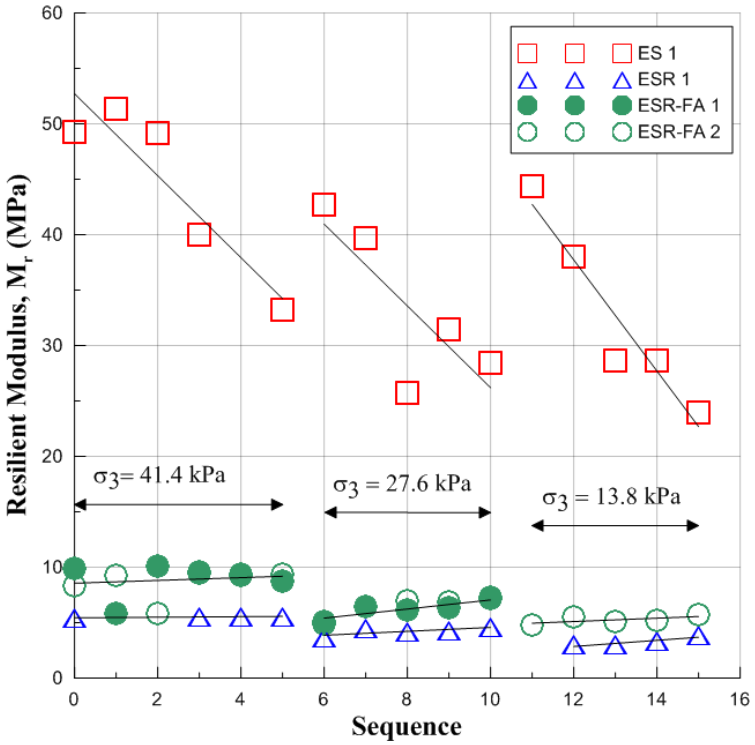

Figure 5.1: Resilient Modulus vs. Sequence Number for ES, ESR, and ESR-FA Specimens

Figure 5.2 shows the variation of the resilient modulus with increasing confining stress. As discussed in the previous paragraph, it is expected that the stiffness of the specimen will increase with increasing confining stress because the confining stress provides additional support to the specimen (US Department of Transportation 2002). Figure 5.3 plots the same data shown in Figure 5.2 except that the expansive soil is not displayed, to provide a better comparison between the ESR and ESR-FA responses.

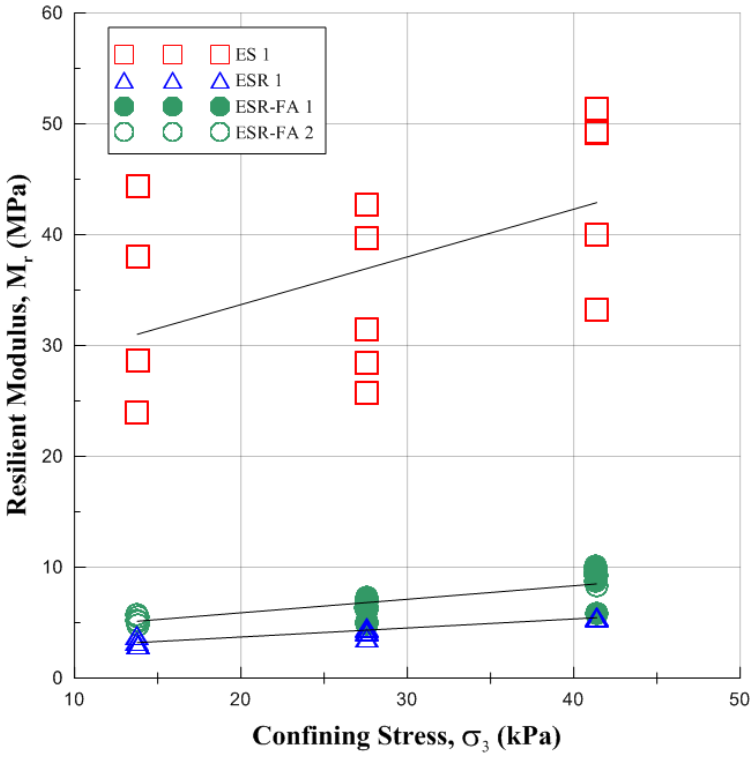

Figure 5.2: Resilient Modulus vs. Confining Stress for ES, ESR, and ESR-FA Specimens

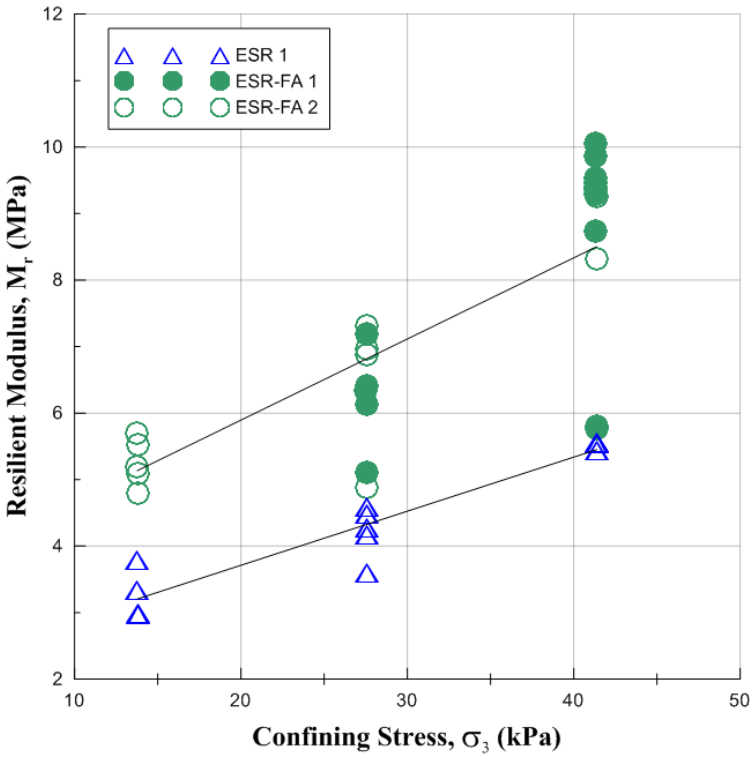

Figure 5.3: Resilient Modulus vs. Confining Stress for ESR, and ESR-FA Specimens

Figure 5.4 displays the variation of the resilient modulus with increasing deviator stress for the expansive soil, ESR, and ESR-FA specimens tested. Figure 5.4 shows that stiffness of the expansive soil decreases as the deviator stress increases. This is expected because the increase in deviator stress causes permanent damage to the specimen and therefore reduces the stiffness (Thompson 1987, US Department of Transportation 2002). However, this is not the case for the ESR and ESR-FA specimens. The stiffness of the ESR and ESR-FA specimens remains essentially constant as the deviator stress increases, which suggests that the permanent damage caused by the deviator stress is small due to the rubber particles in the ESR and ESR-FA specimens.

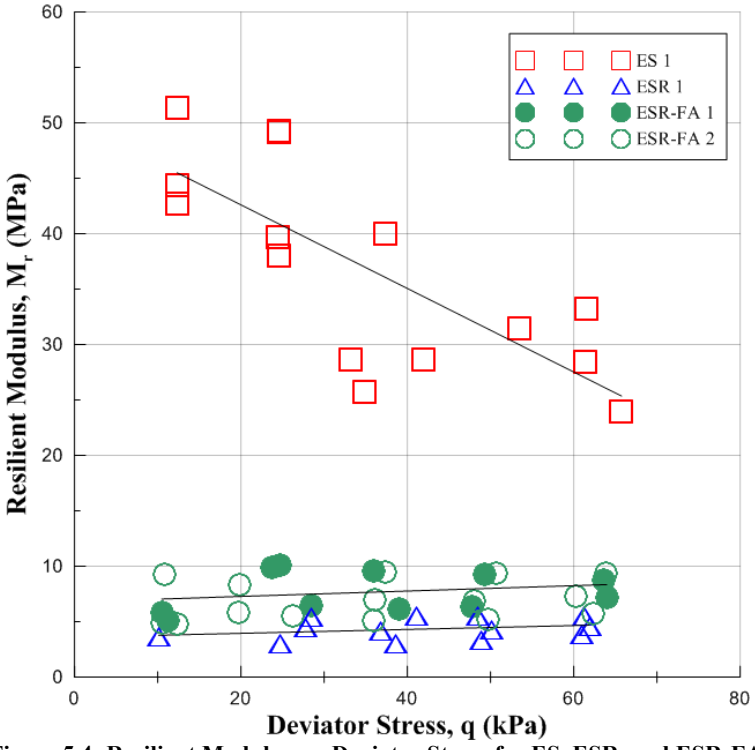

Figure 5.4: Resilient Modulus vs. Deviator Stress for ES, ESR, and ESR-FA

5.1.2 Poisson's Ratio

The results of the Poisson's Ratio tests for the expansive soil, ESR, and ESR-FA are displayed in Figures 5.5, 5.6, and 5.7.

Figure 5.5 displays the variation of deviator stress with the axial strain for the expansive soil, ESR, and ESR-FA specimens tested. As expected, the ESR specimen deformed more than the expansive soil and ESR-FA specimens because the stiffness of the ESR specimen has been shown to be less than that of the expansive soil and ESR-FA specimens (Wiechert 2011, Dunham-Friel 2009). The relationship between the expansive soil and ESR-FA specimens is more complex. The ESR-FA was expected to have a similar response to that of the expansive soil because of the research conducted by Wiechert (2011). Figure 5.5 shows that the initial stiffness of the ESR-FA is similar to the initial stiffness of the expansive soil, which supports research conducted by Wiechert (2011). The expansive soil specimen displays a higher stiffness than the ESR-FA specimen for axial strains ranging from 0 to 3%. Once the axial strain is greater than 3%, the ESR-FA specimen displays a higher stiffness than the expansive soil specimen. A possible irrecoverable yield of the pozzolanic bonds in the ESR-FA specimen may be seen around an axial strain slightly less than 0.5%, after which the stress-strain response of the ESR-FA deviates from and remains below the expansive soil response until an axial strain of about 3% is reached.

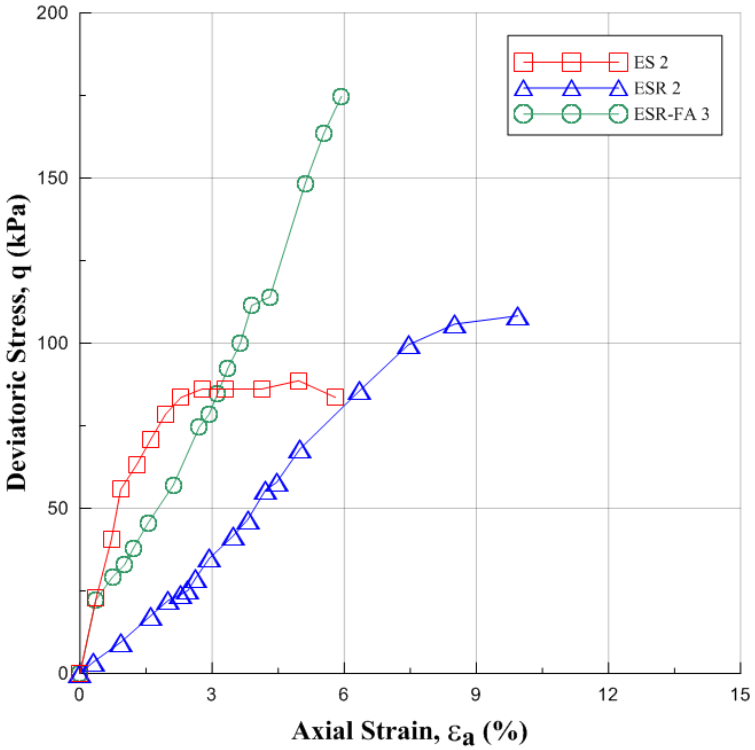

Figure 5.5: Deviator Stress vs. Axial Strain for Poisson's Ratio Tests on ES, ESR, and ESR-FA

Figure 5.5 also presents the elastic response of the material (i.e. the linear portion of the q vs. e_a curve). The axial strain range for the expansive soil, ESR, and ESR-FA are 0% to 0.9%, 0% to 7.5%, and 0% to 4.3%.

Although Figure 5.5 shows a similar stress-strain response between the expansive soil and ESR-FA specimens, this is not the case in Figure 5.6, which presents the variation of Poisson's ratio with axial strain. This plot shows that the ESR-FA behavior is between the expansive soil and ESR. The Poisson's ratio range that represents the elastic response for the specimens can be determined from the Poisson's ratio values that fall in the axial strain ranges discussed in the previous chapter. The Poisson's ratio range that represents the elastic response for the expansive soil, ESR, and ESR-FA specimens are 0.3 to 0.4, 0.1 to 0.2, and 0.1 to 0.3. A slight decrease and

then increase in Poisson's ratio values for the ESR-FA specimen can be seen in Figure 5.6 around an axial stain of 1.5%, which could be due to breakage of cementation.

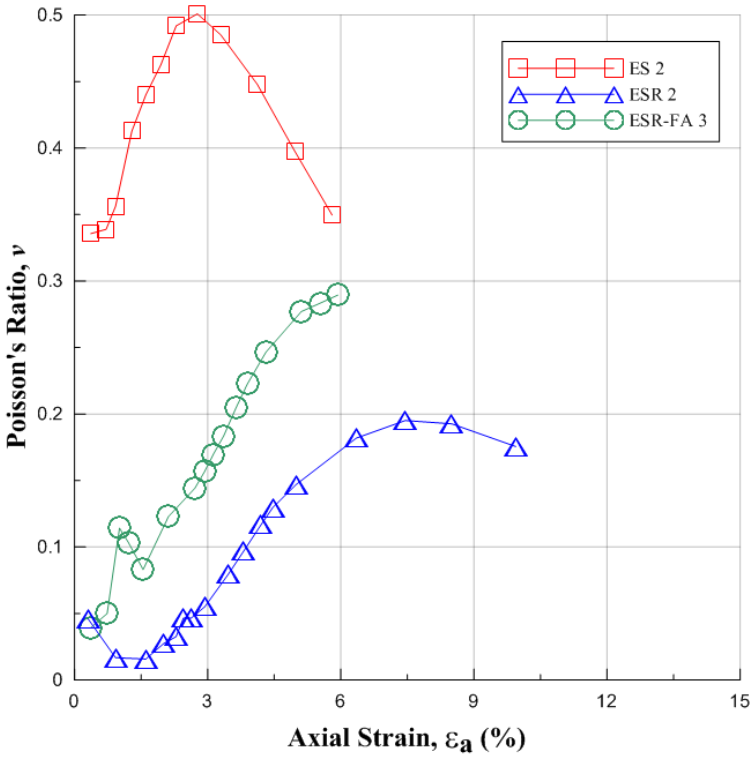

Figure 5.6: Poisson's Ratio vs. Axial Strain for ES, ESR, and ESR-FA

Figure 5.7 presents the variation of radial strain with axial strain. Both the ESR and ESR-FA specimens seem to compress vertically without expanding horizontally between axial strains of 0 to 1.5%. This could be a result of the fabric created by rubber inclusion where the rubber compresses on itself. At any level of axial strain, the ESR presents the lowest amount of radial expansion whereas the expansive soil expands the most along the radial direction. The ESR-FA response is somewhere in between the expansive soil and ESR responses. These responses are consistent with the average values of Poisson's ratio that can be determined from Figure 5.6 as approximately 0.34, 0.14, and 0.1 for the expansive soil, ESR-FA, and ESR, respectively.

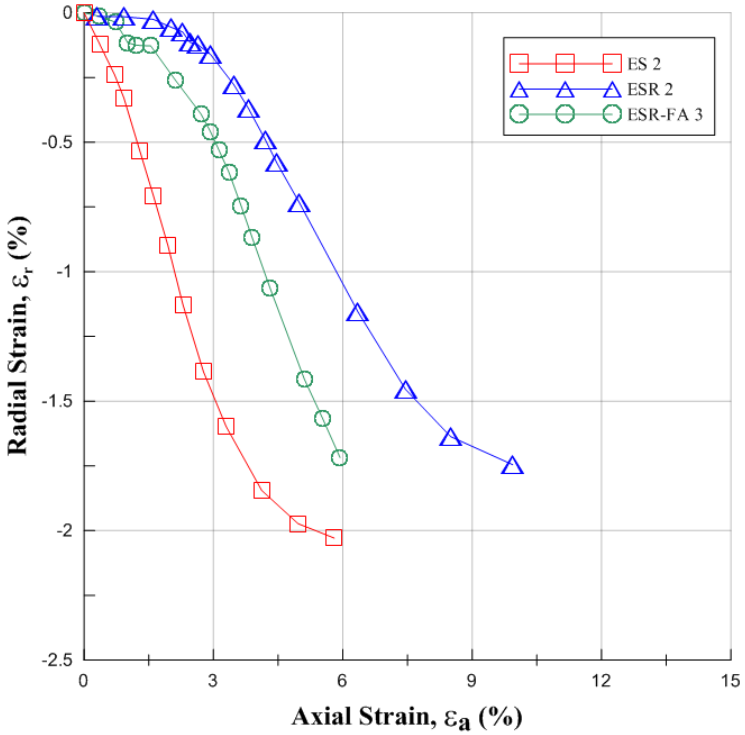

Figure 5.7: Radial Strain vs. Axial Strain for Poisson's Tests on ES, ESR, and ESR-FA

The resilient modulus values used for the computer simulations, which will be discussed in the next section, were determined by taking an average of the resilient modulus values from each of the 15 sequences for each material tested. The Poisson's ratio values for the materials were determined as follows:

- First an axial strain range determined from Figure 5.5 that identifies the initial linear response of the expansive soil, ESR, and ESR-FA specimens (e.g. the axial strain range for the expansive soil is 0.4% to 0.9%, for the ESR is 0.3 to 7.5, and the ESR-FA is 0.4% to 4.3%);
- Once the axial strain range was determined, the average Poisson's ratio that would correspond to that axial range was then determined from Figure 5.6 and used as the materials Poisson's ratio. Table 5.2 displays the parameters used for the computer simulations.

Table 5.2: Material parameters used in computer simulations

Material	STRUCTURAL INFORMATION			
	Resilient Modulus	Poisson's Ratio	Layer Thickness	Slip Condition
	(MPa)		(cm)	
ES	43	0.34	Varied	1
ESR	6	0.10	Varied	1
ESR-FA	9	0.14	Varied	1

5.2 Computer Simulations

Please note that there are three scenarios analyzed in this section. These three scenarios were previously described in Chapter 4, Section 4.2.1 and are also listed below for convenience:

4. Asphalt concrete over expansive soil

    1.A. Asphalt concrete over expansive soil base over expansive soil subgrade

    1.B. Asphalt concrete over expansive soil subgrade

5. Asphalt concrete over ESR base over expansive soil subgrade

6. Asphalt concrete over ESR-FA base over expansive soil subgrade

As a reference, it should be noted that the scenario 1 (AC placed directly on expansive soil) option is not feasible from a practical point of view as such pavement structure would foil due to excessive heave induced by the untreated expansive soil subgrade.

Two critical locations were analyzed in the computer simulations. The first critical location (FCL) was situated at the bottom of the asphalt concrete layer. The second critical location (SCL) was situated at the top of the subgrade layer. A diagram of the critical locations can be seen in Figure 3.10.

An imaginary expansive soil base layer was used in the computer simulations for scenario 1.A (asphalt concrete over expansive soil base over expansive soil subgrade) in order to keep scenarios 1.A, 2, and 3 as similar as possible. Furthermore, by creating this expansive soil base layer for scenario 1.A the SCLs for scenarios 1.A, 2, and 3 were all located at the same depth. However, even though this expansive soil base layer had to be created for the computer simulations, scenario 1.A is still asphalt concrete over expansive soil because the expansive soil base and expansive soil subgrade are the exact same material. This imaginary expansive soil base layer only effects the SCL, and not the FCL. Take note for the analysis in Section 5.2.1 that the vertical displacement, vertical and horizontal normal mircostrain and normal stress of the FCL for scenario 1.A stays constant with increasing base thickness because base thickness is negligible since the base and subgrade are the same material.

Scenario 1.B (Asphalt concrete over expansive soil subgrade) is not discussed in Sections 5.2.1 and 5.2.3, but are discussed in Sections 5.2.2 and 5.2.4. This is because Sections 5.2.1 and 5.2.3 are analyses using the FCL, and since scenario 1.A and 1.B have the same FCL there is no need to analyze scenario 1.B when scenario 1.A is already being analyzed. However, Sections 5.2.2 and 5.2.4 are analyses using the SCL, and since scenario 1.A and 1.B have different SCLs both of them are analyzed. Please note that scenario 1.B is a two layered pavement structure (asphalt concrete over expansive soil subgrade), and since the SCL will always be located at the top of the subgrade there will only be one data point analyzed.

5.2.1 Analysis of the First Critical Location

The vertical displacement (in mm) of the FCLs after the total number of load applications had been applied is presented in Figure 5.8 for all scenarios tested. The FCL of the structure with an ESR base developed the largest displacement. This was expected because the ESR base had the lowest resilient modulus causing its FCL to have a larger vertical normal microstrain and than the expansive soil and ESR-FA base counterparts, as shown in Figure 5.9. Figure 5.8 also shows that the displacement of the FCL above the ESR and ESR-FA bases increase as the thickness of the base layers increases. This is because Weslea calculates the displacement of the critical locations according to the multilayer linear elastic theory. Furthermore, the original base thickness or depth to the subgrade is incorporated when calculating the displacement of the FCL. This linearly correlates the displacement of the FCL to the base thickness, which is why the displacement of the FCL increases as the base thickness increases.

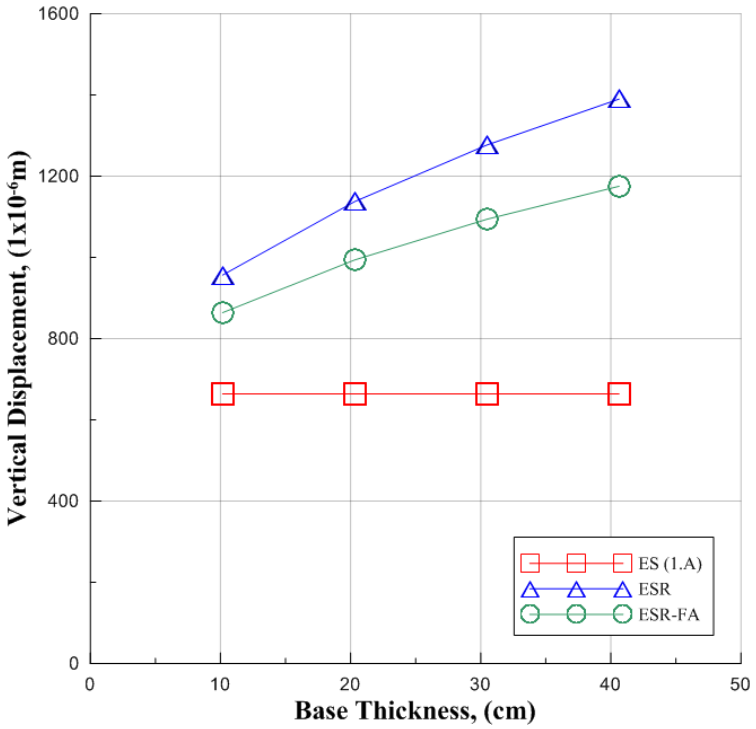

Figure 5.8: Variation of Vertical Displacement with Increasing Base Thickness for the First Critical Location

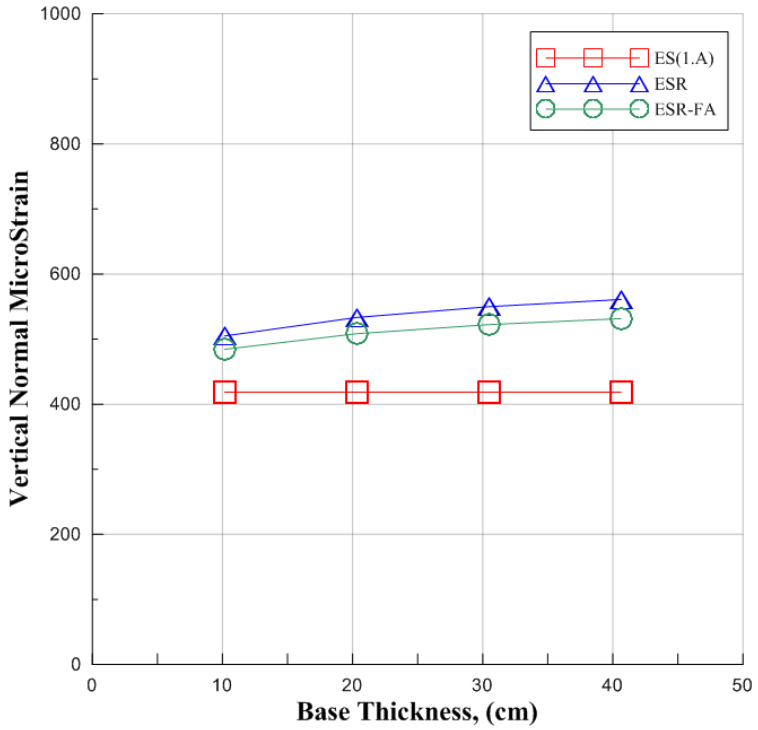

Figure 5.9: Variation of Vertical Normal MicroStrain with Increasing Base Thickness for the First Critical Location

The vertical normal stress applied to the FCLs above the expansive soil, ESR, and ESR-FA bases are displayed in Figure 5.10. The FCL above the expansive soil base has the highest vertical normal stress because it has the highest resilient modulus. The FCL above the ESR base has the lowest vertical normal stress because it has the lowest resilient modulus. The vertical normal stress applied to the FCL above the ESR and ESR-FA bases decreases as the base thickness increases because of the change in the stress distribution. Weslea analyzes stress distribution using the multilayer linear elastic theory. When calculating the vertical stress at the bottom of the asphalt concrete layer the depth to the subgrade is incorporated. Therefore, by increasing the base thickness the depth used in the stress distribution analyses is also increased.

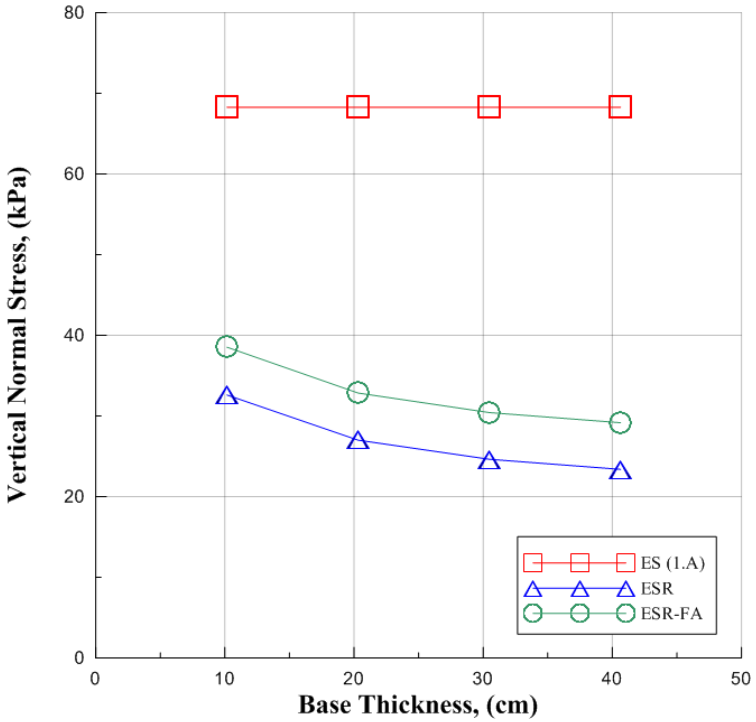

Figure 5.10: Variation of Vertical Normal Stress with Increasing Base Thickness for the First Critical Location

The horizontal normal microstrain and normal stress of the FCLs are displayed below in Figures 5.11 and 5.12. The values of the horizontal normal microstrain and normal stress are negative, which means that the strains and stresses are tensile. Figure 5.11 shows that the FCL above the ESR base has the highest horizontal normal microstrain, and the FCL above the expansive soil base has the lowest horizontal normal microstrain, which is due to the fact that the ESR has the lowest resilient modulus and the expansive soil has the highest resilient modulus. As the base thickness increases, the horizontal normal microstrain for the FCLs above the ESR and ESR-FA bases increase in magnitude. This is because the horizontal normal stress of the FCLs above the ESR and ESR-FA bases also increases as the base thickness increases. The reason the horizontal normal stress increases is because by increasing the ESR and ESR-FA base thicknesses the expansive soil subgrade, which is a stiffer material, is being replaced by a material that has a lower resilient modulus.

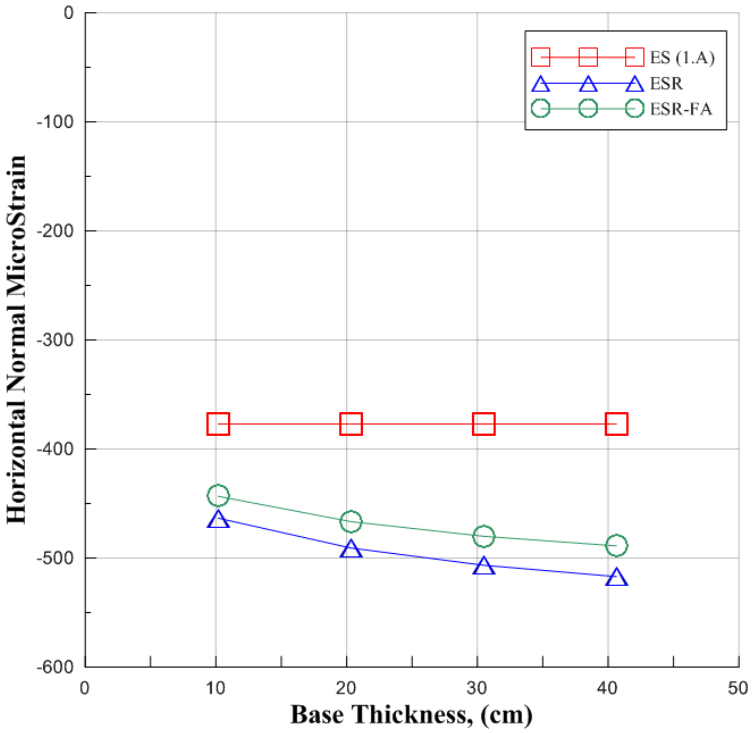

Figure 5.11: Variation of Horizontal Normal MicroStrain with Increasing Base Thickness for the First Critical Location

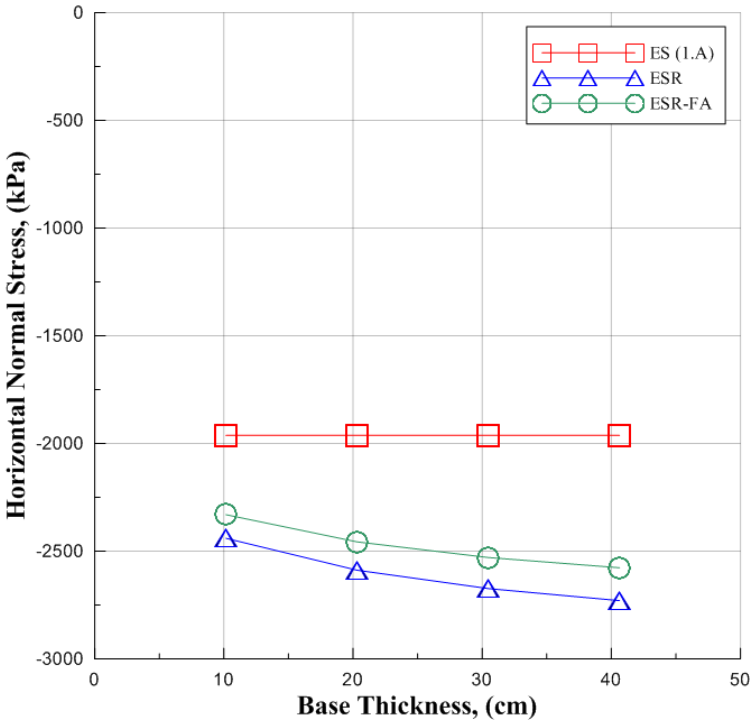

Figure 5.12: Variation of Horizontal Normal Stress with Increasing Base Thickness for the First Critical Location

5.2.2 Analysis of the Second Critical Location

The SCL is always located in expansive soil because it is located at the top of the subgrade layer. The base (second layer) is the variable layer that was simulated as expansive soil, ESR, or ESR-FA.

Please note that the SCL analyzed in this section for scenario 1.B always has a slightly greater magnitude than the SCLs analyzed for scenario 1.A. This is because the SCL for scenario 1.B is located at the top of the subgrade, or directly beneath the asphalt concrete layer. Furthermore, the SCLs for scenario 1.A are located a greater depth into the ground than the SCL for scenario 1.B, and because the SCL for scenario 1.B is located closer to the surface it has a greater vertical normal stress applied to it. Since the SCL for scenario 1.B has a greater vertical normal stress applied to it, the magnitude of the horizontal normal stress, vertical and horizontal normal mircostrain, and vertical displacement will also be greater in magnitude than the SCLs for scenario 1.A.

Figure 5.13 shows the SCL beneath the expansive soil base with the highest vertical displacement, and the SCL beneath the ESR base with the lowest amount of vertical displacement. The SCL had the largest amount of vertical displacement when the expansive soil was used as the base because the expansive soil base applied a larger vertical normal stress (kPa) than the ESR and ESR-FA bases did, which can be seen in Figure 5.14. The SCL underneath the ESR base developed the smallest vertical displacement because the ESR base applied the lowest vertical normal stress (kPa).

Also, as the expansive soil, ESR, and ESR-FA base thicknesses increase, the vertical displacement, normal stress, and normal microstrain of the SCLs beneath the expansive soil, ESR, and ESR-FA bases decrease, which can be seen in Figures 5.13, 5.14, 5.15. This is because the vertical normal stress decreases with increasing depth, and by increasing the thickness of the base layer, the depth of the SCL is also increased.

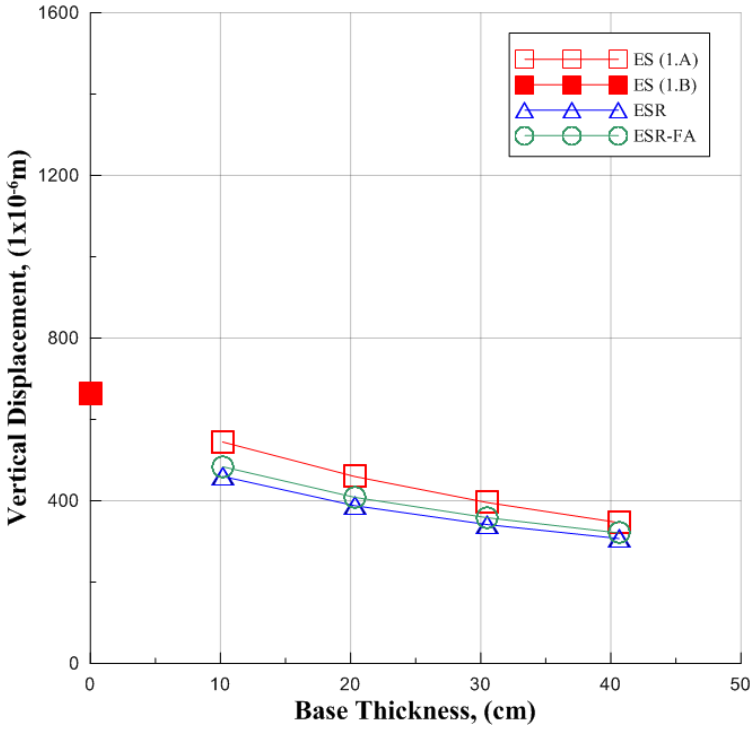

Figure 5.13: Vertical Displacement with Increasing Base Thickness for the Second Critical Location

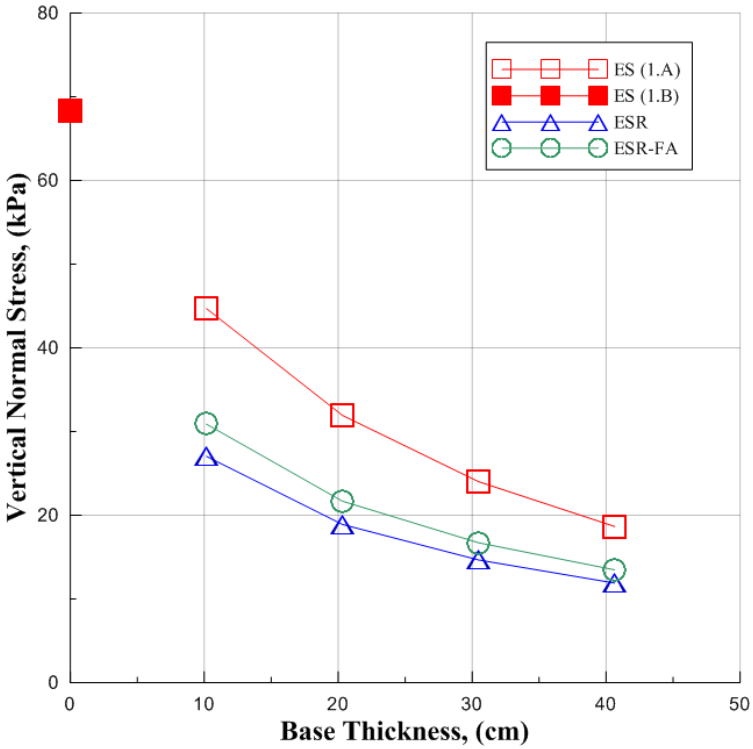

Figure 5.14: Variation of Vertical Normal Stress with Increasing Base Thickness for the Second Critical Location

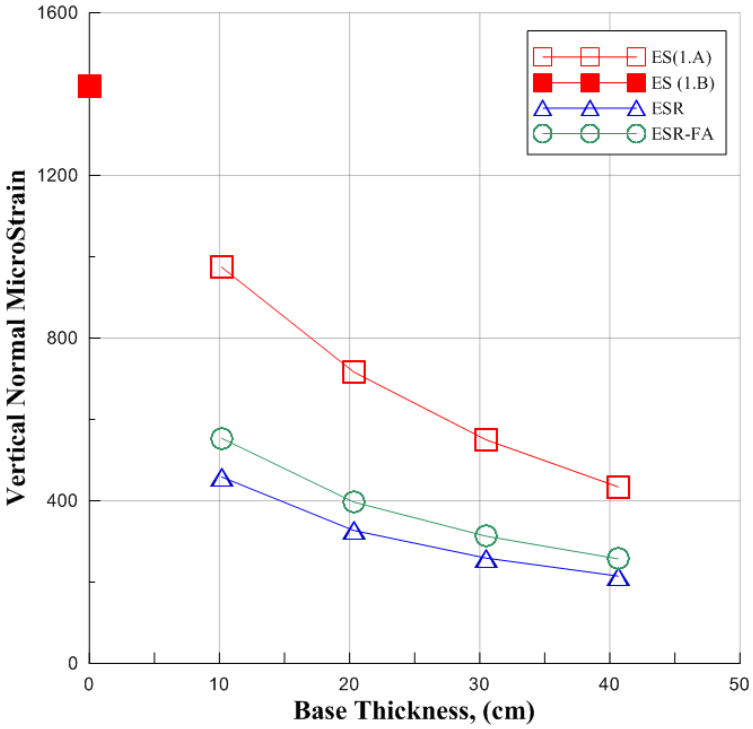

Figure 5.15: Variation of Vertical Normal MicroStrain with Increasing Base Thickness for the Second Critical Location

The horizontal normal microstrain of the SCLs are displayed in Figure 5.16. The values of the horizontal normal microstrain are negative, which means that these are tensile strains. Figure 5.16 shows that the SCL beneath the expansive soil base has the highest horizontal normal microstrain, and the SCL beneath the ESR has the lowest horizontal normal microstrain. This is because the SCL beneath the expansive soil base has the highest vertical normal mircostrain and normal stress, while the SCL beneath the ESR has the lowest vertical normal mircostrain and normal stress. As the base thickness increases, the horizontal normal microstrain of the SCLs beneath the expansive soil, ESR, and ESR-FA bases decrease. This is because the horizontal normal stress of the SCLs also decreases as the base thickness increases, which can be seen in Figure 5.17. The reason the horizontal normal stresses decrease as the base thickness increases is because vertical normal stress decreases as it goes further into the ground. By increasing the base thickness, the depth to the SCL increases, which decreases the vertical normal stress applied to the SCL, and therefor decreases the horizontal normal stress applied to the SCL.

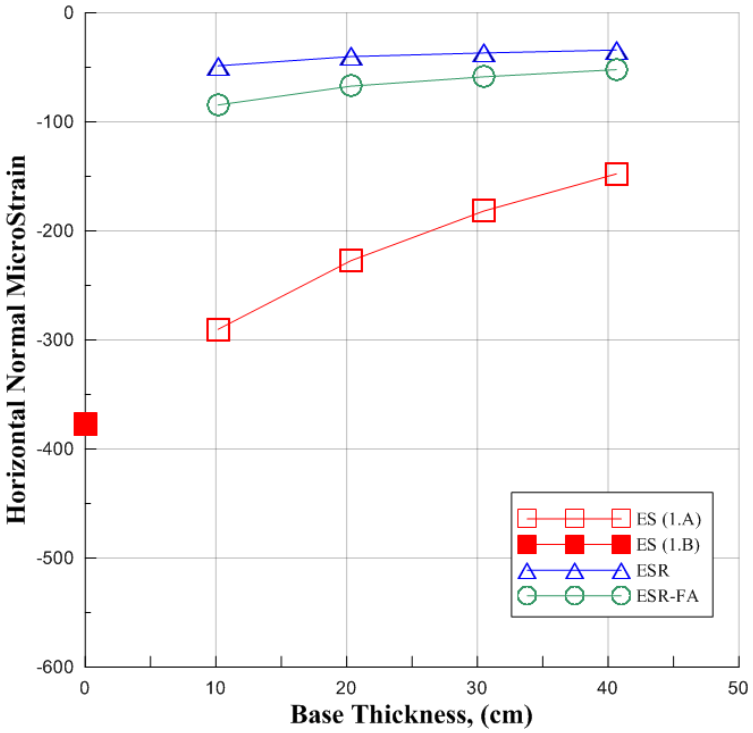

Figure 5.16: Variation of Horizontal Normal MicroStrain with Increasing Base Thickness for the Second Critical Location

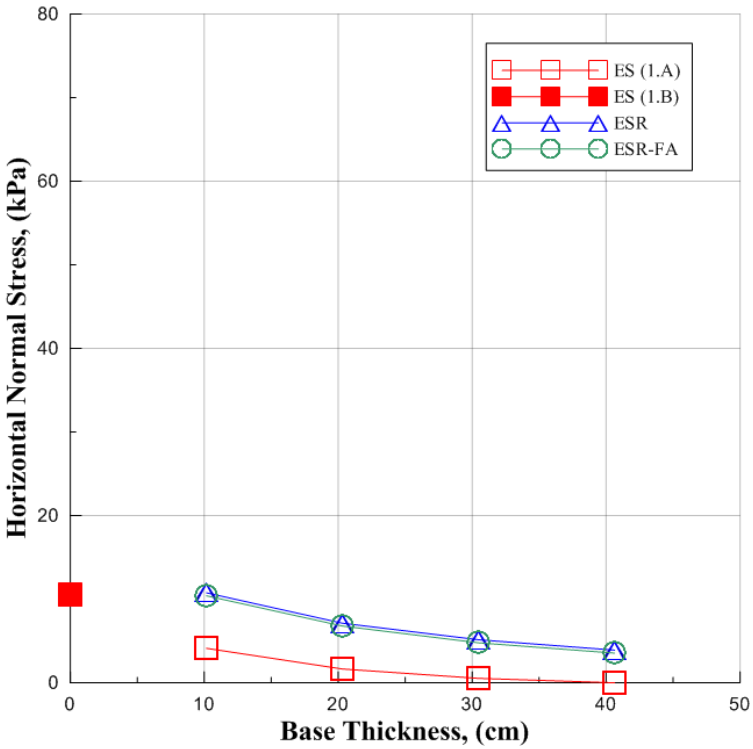

Figure 5.17: Variation of Horizontal Normal Stress with Increasing Base Thickness for the Second Critical Location

5.2.3 Analysis of Fatigue

Weslea software can estimate the number of cycles that can be applied to the pavement structure before fatigue and rutting occur, which is referred to as the number of cycles allowed. The number of cycles allowed before fatigue occurs is determined using Equation 3.13, and the number of cycles allowed before rutting occurs is determined using Equation 3.14. A damage ratio, which is defined as the ratio of number of the cycles applied to number of cycles allowed, is also supplied in the output data. A default value of 1000 applied cycles was used for all simulations.

Figure 5.18 displays the number of allowed cycles that can be applied to the pavement structure before fatigue occurs. As the ESR and ESR-FA base thicknesses increase, the number of cycles allowed before fatigue occurs decreases. This is because the ESR and ESR-FA base layers have a lower stiffness than the expansive soil subgrade. As the ESR and ESR-FA base layer thickness increase, the pavement structure as a whole become less stiff. However, the ESR-FA base has a longer life (number of cycles allowed) than the ESR base, which confirms that the addition of fly ash improves the life of ESR mixtures. Figure 5.18 shows scenario 1 with the longest life (number of cycles allowed), which is because the FCL above the expansive soil has the lowest maximum horizontal tensile strain as a result of the expansive soil having the highest resilient modulus.

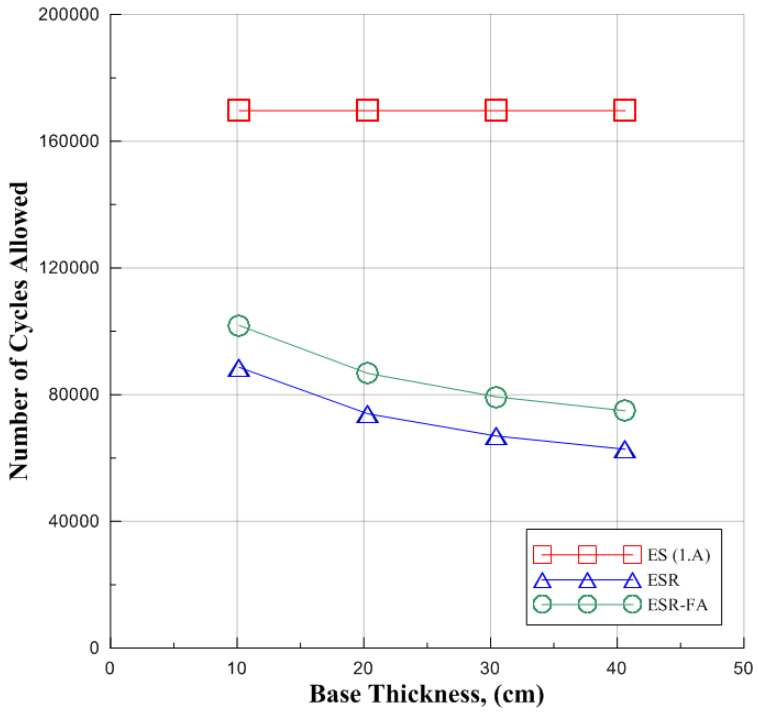

Figure 5.18: Number of Cycles Allowed before Fatigue Occurs as a Function of Base Thickness

The damage ratio for fatigue is 0.01 for pavement structures with expansive soil, ESR, and ESR-FA bases except for the pavement structure with an ESR base that is 40.64 cm thick, which can be seen in Figure 5.19. This is because as the number of cycles allowed decreases the damage ratio increases. However, the number of cycles allowed are dramatically greater than the number of cycles applied causing the increase in the damage ratio to be so minimal that it is not seen until the base thickness is 40.64 cm.

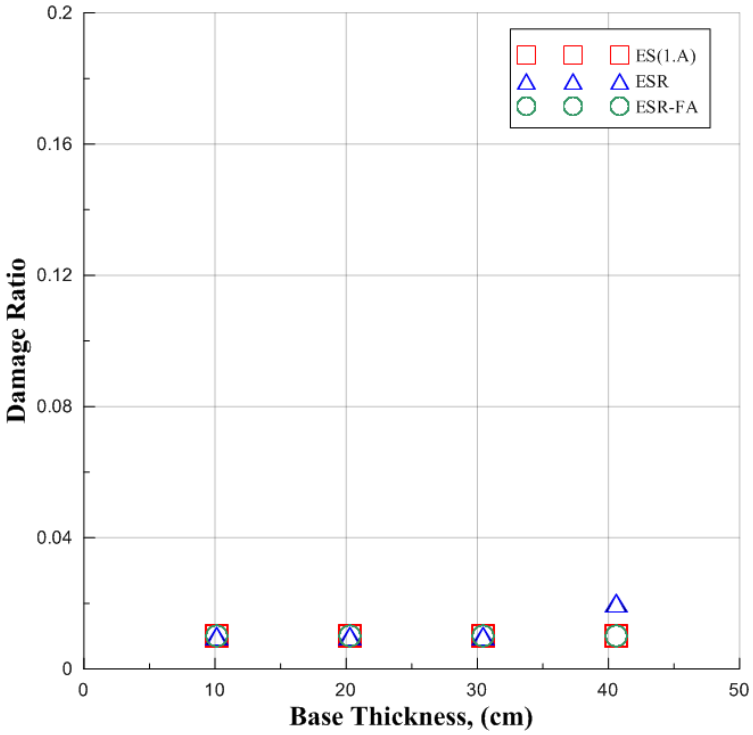

Figure 5.19: Fatigue Damage Ratio in Comparison with Base Thickness

The fatigue analysis results suggest that scenario 1 (asphalt concrete over expansive soil) is the best choice for a pavement structure. However, since scenario 1 is not feasible from a practical point of view as such pavement structure would hinder due to excessive heave induced by the untreated expansive soil subgrade, the author suggests scenario 3 (asphalt concrete over ESR-FA over expansive soil subgrade) as the better pavement structure.

5.2.4 Analysis of Rutting

Figure 5.20 displays the number of allowed cycles that can be applied to the pavement structure before rutting occurs. Take note that the number of cycles allowed before rutting occurs is determined using the maximum vertical compressive strain at the top of the subgrade (second critical location). Figure 5.20 shows that as the base thickness increases for all three pavement

structures the number of allowed cycles increases. This is because as base thickness increases the second critical location goes further into the ground, and stress and strain decrease with depth. Figure 5.20 shows that the ESR base allows the highest number of cycles allowed. This is because the SCL beneath the ESR base has the lowest maximum vertical compressive strain.

Please not that the actual number of cycles allowed for scenario 1 are the number of cycles allowed for scenario 1.B, which are significantly less than the number of cycles allowed for scenario 2 and 3.

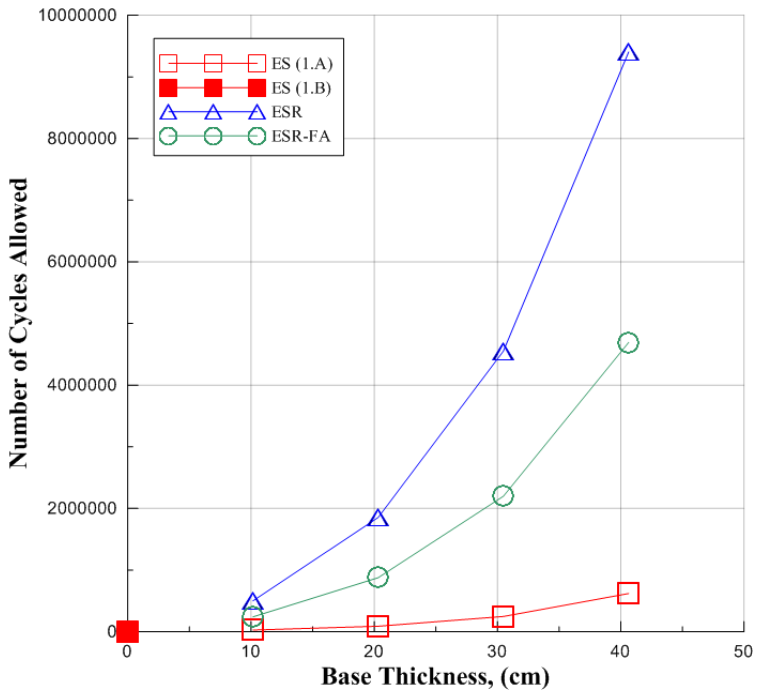

Figure 5.20: Number of Cycles Allowed before Rutting Occurs as a Function of Base Thickness

The damage ratio for rutting is zero for pavement structures with ESR and ESR-FA bases, which can be seen in Figure 5.21. This is because the number of cycles allowed are dramatically greater than the number of cycles applied for pavement structures with ESR and ESR-FA bases, which

causes the damage ratio to be so minimal that it is basically equal to zero. Pavement structures with expansive soil bases in scenario 1.A that are 10.16 and 20.32 cm thick have a damage ratio of 0.04 and 0.01. This is because as the number of cycles allowed increase the damage ratio decreases. Furthermore, as the base thickness increases the strains at the second critical location decrease, which increase the number of cycles allowed and decreases the damage ratio. The pavement structure for scenario 1.B has a damage ratio of 0.16. Please not that the actual damage ratio for scenario 1 is the damage ratio for scenario 1.B, which is significantly greater than the damage ratios for scenario 2 and 3.

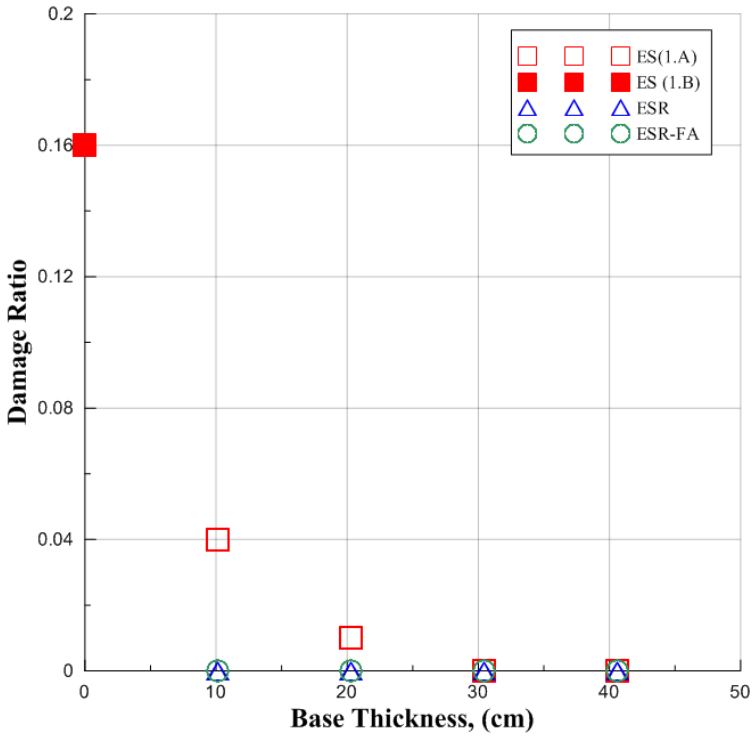

Figure 5.21: Rutting Damage Ratio in Comparison with Increasing Base Thickness

These results suggest that scenario 2 (asphalt concrete over ESR base over expansive soil subgrade) is the best choice for a pavement structure. However, because the stiffness of the ESR material is so low, the author suggests scenario 3 (asphalt concrete over ESR-FA over expansive soil subgrade) as the better pavement structure.

CHAPTER 6. **CONCLUSIONS**

6.1 Research Objectives

The first objective on this research was to conduct resilient modulus tests on a select ESR mixture stabilized with off-specification fly ash (ESR-FA). The second objective of this research was to asses the Poisson's ratio of expansive soil, ESR and ESR-FA mixtures. Thirdly, evaluate the fatigue and rutting performance of pavement base layers of expansive soil, ESR, and ESR-FA using a computer program.

6.2 Resilient Modulus

Based on research conducted by Wiechert (2011) the resilient modulus of the ESR-FA specimen should have been greater than or equal to the resilient modulus of the expansive soil specimen. The results of this study show that the addition of the fly ash to the ESR mixture did improve the stiffness of the ESR specimen. Furthermore, the resilient modulus of the ESR-FA specimen was greater than the ESR specimen. However, the addition of fly ash did not improve the stiffness of the ESR mixture enough to obtain stiffness equal to or greater than the expansive soil mixture. One reason the expansive soil specimen's resilient modulus was greater than the ESR-FA specimen's resilient modulus could be that not enough pozzolanic bonds formed in the ESR-FA specimen. Another reason the results of this study differ from Wiechert (2011) could be due to the nature of the load (cyclic vs. static).

6.3 Poisson's Ratio

Poisson's ratio tests were conducted on expansive soil, ESR, and ESR-FA specimens. The expansive soil specimen had the highest Poisson's ratio equaling 0.34, and the ESR specimen had the lowest Poisson's ratio equaling 0.10. This means that the expansive soil specimen had a greater radial expansion when undergoing vertical compression than the ESR specimen. The ESR-FA specimen had a Poisson's ratio between the expansive soil and ESR specimens equaling 0.14. However, the Poisson's ratio of the ESR-FA specimen was closer to the ESR specimen than the expansive soil specimen. The reason the ESR and ESR-FA specimens did not have as great of a radial expansion could be a result of the fabric created by rubber inclusion where the rubber compresses on itself.

6.4 Computer Simulations

When analyzing fatigue, scenario 1 (asphalt concrete over expansive soil) had the longest life span (highest number of cycles allowed) and the lowest damage ratio, which is because the FCL above the expansive soil has the lowest maximum horizontal tensile strain as a result of the expansive soil having the highest resilient modulus. The results from the fatigue analyses suggest that scenario 1 is the best choice for a pavement structure as far as fatigue is concerned. However, since scenario 1 is not feasible from a practical point of view, as such pavement structure would fail due to excessive heave induced by the untreated expansive soil subgrade, the author suggests scenario 3 (asphalt concrete over ESR-FA over expansive soil subgrade) as the recommended pavement structure of the three scenarios.

When analyzing rutting, scenario 2 (asphalt concrete over ESR base over expansive soil subgrade) had the longest life span (highest number of cycles allowed) and the lowest damage ratio, which is because the SCL beneath the ESR base has the lowest maximum vertical compressive strain as a result of the ESR base having the lowest resilient modulus. The results from the rutting analyses suggest that scenario 2 (asphalt concrete over ESR base over expansive soil subgrade) is the best choice for a pavement structure compared to scenarios 1 and 3. However, because the stiffness of the ESR material is so low, the author suggests scenario 3 (asphalt concrete over ESR-FA base over expansive soil subgrade) as the recommended pavement structure of the three scenarios.

In conclusion, when choosing between scenarios 1, 2 or 3, the author suggests scenario 3 as the optimal choice. The reasons scenario 1, and 2 are not feasible are listed below:

1. Scenario 1 is not feasible from a practical point of view, as such pavement structure would fail due to excessive heave induced by the untreated expansive soil subgrade.
2. Scenario 2 has a resilient modulus too low to support a pavement structure.

Therefore, scenario 3 is the optimal choice because the ESR-FA base swell potential is significantly lower than the expansive soil base, and the stiffness of the ESR-FA base is greater than the ESR base.

6.5 Suggestions for Future Work

Based on the results of this study the following suggestions for future work are:

1. Evaluation of resilient modulus tests conducted on expansive soil, ESR, and ESR-FA specimens using an apparatus specifically designed for resilient modulus testing.

2. Conduct studies on ESR-FA specimens with a *RC* less than 20%.
3. Evaluation of the impacts on the environment caused by soils stabilized with off-specification fly ashes.
4. Construction and monitoring of field scale test sections.
5. Evaluation of non-expansive soil stabilized with high sulfur content off-specification fly ashes.

CHAPTER 7. REFERENCES

"2010 Annual Report to the House Transportation legislation review Committee on the Status of Waste Tire Recycling in Colorado." Colorado Department of Public Health and Environment, Denver, 2010.

Ahmed, I., and C. W. Lovell. *Rubber Soils as Lightweight Geomaterials.* Transportation Research Record 1422, 1993.

American Association of State Highway and Transportation Officials. "Determining the Resilient Modulus of Soils and Aggregate Materials." 2003.

American Coal Ash Association. "2009 Coal Combustion Product (CCP) Production & Use Survey Report." *Ash At Work*, no. 2 (2010): 15.

—. "ACAA Advancing the Management and Use of Coal Combustin Products." *ACAA* . 2008. www.acaa-usa.org/diplaycommon.cmf?an=1&subarticlenbr=112 (accessed March 28, 2012).

American Coal Ash Association Education Foundation. *ACAA.* American Coal Ash Association Education Foundation. 2008. www.acaa-usa.org/displaycommon.cfm?an=1&subarticlenbr=109 (accessed March 28, 2012).

Atkinson, J. H. "Non-linear Soil Stiffness in Routine Design." *Geotechnique* 50, no. 5 (2000): 487-508.

Dunham-Friel, Jesse. *Shear Strength and Stiffness of Expansive Soil and Rubber (ESR) Mixtures in Undrained Axisymmetric Compression.* Fort Collins, CO: Colorado State University, 2009.

Edil, Tancer B., Craig H. Benson, and Universtiy of Wisconsin-Madison. "Geotechnical Applications of CCPS in Wisconsin." *Ash at Work* (Lester publications, LLC), Summer 2006: 16-20.

Fox, John; BASF Construction Chemicals, LLC. "Fly Ash Chemical Classification Based on Lime." *Ash at Work* (Lester Publications, LLC), no. 1 (2007): 28.

Hilt, G.H., and D.T. Davidson. "Lime Fixation in Clayey Soils." *Highway Research Board*, 1960.

Holtz, R.D., and W.D. Kovacs. *An Introduction to Geotechnical Engineering.* Upper Saddle River, NJ: Prentice Hall, 1981.

Huang, Yang H. *Pavement Analysis and Design.* 2nd. New Jersey: Pearson Prentice Hall, 2004.

Kim, H. K., and J. C. Santamarina. "Sand-rubber Mixtures (Large Rubber Chips)." *Can. Geotech*, 2008: 1457-1466.

Lee, J. H., R. Salgado, A. Bernal, and C. W. Lovell. "Shredded Tires and Rubber-Sands as Lightweight Backfill." *Journal of Geotechnical and Geoenvironmental Engineering*, 1999: 132-141.

Lee, J. S., J. Dodds, and J. C. Santamarina. "Behavior of Rigid-Soft Particle Mixtures." *Journal of Materials in Civil Engineering*, 2007: 179-184.

Nelson, J. D., and D. J. Miller. *Expansive Soils: Problems and practice in foundation and pavement engineering.* New York: John Wiley and Sons, 1992.

Olive, W. A., A. C. Chleborad, C. J. Frahme, J. R. Shlocker, R. Schneider, and R. Schuster. "Swelling Clays Map of the Conterminous United States." *USGS Miscellaneous Investigation Series.* Vols. Map I-1940. 1989.

Ozkul, Z. H., and G. Baykal. "Shear Behavior of Compacted Rubber Fiber-Clay Composite in Drained and Undrained Loading." *Journal of Geotechnical and Geoenvironmental Engineering*, 2001: 767-781.

Pupalla, Anand J., and Amy Cerato. "Heave Distress Problems in Chemically-Treated Sulfate-Laden Materials." *Geo-Strata* 10, no. 2 (March/April 2009): 28-30.

Rubber Manufactures Association. "Scrap Tire Markets in the United States." 2006.

Rubber Manufactures Association. *Scrap Tire Markets in the United States 9th Biennial Report.* Rubber Manufactures Asscoiation, 2009.

"Scrap Tire Cleanup Guidebook." *U.S. EPA.* 2006. (accessed 2012).

Scrap Tire Markets in the United States. 2012. www.rma.org/scrap_tires (accessed May 10, 2012).

Scrap Tire Markets in the United States. 2009. www.rma.org/scrap_tires (accessed May 10, 2012).

Seda, J. H., L. C. Joon, and J. A. Carraro. "Benificial Use of Waste Tire Rubber for Swelling Potential Mitigation in Expansive Soils." *Geotechnical Special Publication 172.* Denver: American Society of Civil Engineers, 2007.
—. "Benificial Use of Waste Tire Rubber for Swelling Potential Mitigation in Expansive Soils." *Geotechnical Special Publication 172.* Denver: American Society of Civil Engineers, 2007.

Thompson, M. R. "ILLI-PAVE BASED FULL-DEPTH ASPHALT CONCRETE PAVEMENT DESIGN PROCEDURE." *The University of Michigan Sixth International Conference Structural Desigh of Asphalt Pavements.* Michigan, 1987.

Timm, Dave, Bjorn Birgisson, and Dave Newcomb. *Weslea for Windows.* 3rd. Septmenber 1999.

U.S. Environmental Protection Agency. "High-Volume Use of High-Carbon Fly Ash for Highway Construction. Case Study 21." U.S. Enviromental Protection Agency, 2008.

U.S. Environmental Protection Agency. "Using Coal Ash in Highway Construction: A Guide to Benefits and Impacts." EPA, 2005.

Wiechert, Ethan Patrick. *Beneficial Use of Off-Specification Fly Ashes to Increase the Shear Strength and Stiffness of Expansive Soil-Rubber (ESR) Mixtures.* Fort Collins, CO: Colorado State University, 2011.

—. *Beneficial Use of Off-Specification Fly Ashes to Increase the Shear Strength and Stiffness of Expansive Soil-Rubber (ESR) Mixtures.* Fort Collins, CO: Colorado State University, 2011.

Wood, David Muir. *Soil Mechanics A One-Dimensional Introduction.* 1. Cambridge University Press, 2009.

Wykeham Farrance. *Dynamic Hollow Cylinder Apparatus.* Wykeham Farrance. 2006.

Wykeham Farrance. *Dynamic Hollow Cylinder System Proposal.* Wykeham Farrance. 2006.